



Observer-based interval type-2 fuzzy friction modeling and compensation control for steer-by-wire system

Gang Luo¹ · Zezheng Wang² · Bingxin Ma¹ · Yongfu Wang¹ · Jianfeng Xu³

Received: 17 June 2020 / Accepted: 5 February 2021 / Published online: 12 March 2021
© The Author(s), under exclusive licence to Springer-Verlag London Ltd. part of Springer Nature 2021

Abstract

This paper studies the tracking control of the SbW system with unknown nonlinear friction torque and the unmeasured angular velocity. An observer-based adaptive interval type-2 fuzzy logic system controller is proposed to eliminate the adverse influence of the friction torque on the SbW system. Firstly, the angular velocity of the front wheels is estimated via the observer, such that the system sensitivity to measurement noise, the hardware cost, and the structural complexity are reduced. Then, an interval type-2 fuzzy logic system (IT2 FLS) is used to model the friction torque, in which the model and parameters are not effectively identified. IT2 FLS has a more exceptional ability to deal with uncertainties than the traditional type-1 fuzzy logic system (T1 FLS), so the friction modeling based on IT2 FLS has more satisfactory effect in practical application. Finally, an adaptive interval type-2 fuzzy logic system controller is proposed to achieve excellent tracking performance. The tracking error can be guaranteed to converge asymptotically to zero by the Lyapunov stability theory. The numerical simulations and hardware-in-loop (HIL) experiments verify the effectiveness and superiority of the proposed friction modeling method and control strategy.

Keywords Steer-by-wire system · Friction torque · Interval type-2 fuzzy logic system · Observer · Hardware-in-loop

1 Introduction

As one of the most advanced automobile technologies, the autonomous vehicle technique has attracted significant attention from the industrial communities over the past two decades. The Steer-by-wire (SbW) technique is an essential component in the development of self-driving. As a new generation of the steering system, the SbW system possesses the following distinct characteristics compared with the traditional steering system: (1) the mechanical connection between the steering wheel and the front wheels is removed; (2) a steering motor is used to generate torque for the front wheels. The excellent steering performance can guarantee the front wheels of the SbW system accurately track the desired trajectory. As a common and complicated nonlinear physical process, friction phenomena seriously affects the steering performance of the SbW system since it causes tracking error, limit cycle, and abnormal vibration [1]. Therefore, to achieve high steering performance, the influence of nonlinear friction torque on the SbW system should deserve considerable attention [2, 3]. For the steering control research of the SbW system, the technical

✉ Yongfu Wang
yfwang@mail.neu.edu.cn

Gang Luo
m15940256365@163.com

Zezheng Wang
m135122@126.com

Bingxin Ma
bingxinma1710116@126.com

Jianfeng Xu
neu_122@sina.com

¹ School of Mechanical Engineering and Automation, Northeastern University, 110819 Shenyang, Liaoning, China

² School of Automation Science and Electrical Engineering, Beihang University, 100191 Beijing, China

³ State Key Laboratory of Digital Manufacturing Equipment and Technology, Huazhong University of Science and Technology, 430074 Wuhan, China

difficulties mainly include friction modeling and steering angular velocity measurement of the front wheels. Friction modeling methods include mechanism modeling method and intelligent modeling method.

The unavoidable friction phenomena between the tire and the road occurring in the SbW system generally cause the steering performance to deteriorate due to non-negligible tracking errors, limit cycles, abnormal vibration, and undesired stick-slip motion. Control strategies that attempt to compensate for the effects of friction inherently require a suitable friction model to predict and to compensate for the friction. Therefore, friction modeling researches have attracted wide attention from researchers. Generally, the design procedure of the friction compensation control strategy can be divided into two categories: model-based method and mode-free method. The model-based method is to use the friction model for an approximate cancellation of disturbances mainly defined by friction. The compensation performance is highly dependent on the accuracy of the friction model. To accurately describe the dynamic behavior of friction, various friction models have been proposed by numerous researchers. The simple classical, static friction models are described by static mappings between velocity and friction forces, such as Coulomb friction, viscous friction, Stribeck friction. However, the above models explain neither hysteretic behavior when studying friction for nonstationary velocities nor variations in the break-away force with the experimental condition nor small displacements at the contact interface during stiction. Therefore, several dynamic friction models have been proposed over the past decades; like the Dahl model [4], the LuGre model [5], the Leuven model [6], and the generalized Maxwell-slip model [7].

Based on the above friction models, many friction compensation schemes are designed [8–15]. In [8], a cascade control strategy was designed based on the static friction model and the GMS model for a high-speed milling machine. In [9], the model switching feedback compensation control considering the rolling friction characteristics was presented for table drive systems. In [10], a friction compensation method based on the LuGre friction model was proposed to reduce the friction influence in the DC motor. An adaptive backstepping controller based on a continuously differentiable LuGre model was proposed for hydraulic actuators [11]. In [12], a friction compensation method was designed for the mechanical servo system based on the LuGre friction model, in which the parameters were identified by the evolutionary algorithm. Although these controllers in the approaches mentioned above seem to be attractive, the exact mathematical model of the friction is necessarily required. The modeling of friction torque in the SbW system is still a challenge as the strong nonlinearity of the friction and the complicated road

conditions. Although many kinds of friction models are available, there is no unified framework. It is difficult to determine which type of friction model is more suitable for a specific task in practice. The simplified friction models can be easily implemented for control compensation, but it is hard to guarantee the tracking accuracy of the control systems. While more sophisticated friction models can result in better control performances, they are more challenging to implement due to the optimization of model parameters.

To solve the difficult problem of the above mechanism modeling methods, the mode-free technique based on intelligent modeling technologies such as fuzzy logic system has attracted considerable interest in friction compensation control. Fuzzy logic system (FLS) can uniformly approximate nonlinear continuous functions to arbitrary accuracy and has been found to be particularly useful to model unknown functions in nonlinear systems [16–20]. Reference [21] proposed a proportional derivative controller with a friction compensation term constituted by a FLS to ensure the control performance of the 1-DOF robot system. In [22], a FLS was used to approximate the model of permanent magnet synchronous machines with nonlinear friction, and then an adaptive control strategy was introduced to obtain high control accuracy. In [23], the authors employed a FLS to approximate the friction in the networked teleoperation system, then a finite-time synchronization control method was designed. In [24], a FLS was used to model the uncertain friction force in multi-axis servo systems. It is worth mentioning that the FLS adopted in the above investigations is the type-1 fuzzy logic system (T1 FLS). The fuzzy sets in T1 FLS are type-1 fuzzy sets (T1 FSs), which have accurate membership functions. The accurate membership functions have limitations in dealing with the unknown friction with strong uncertainty [25, 26]. To address this problem, an adaptive controller based on interval type-2 fuzzy logic system (IT2 FLS) is proposed in this study.

Type-2 fuzzy logic system (T2 FLS), which is a FLS that uses at least one Type-2 fuzzy set (T2 FS), has become a hot research issue. T2 FS is an extension of the concept of the traditional type-1 fuzzy set (T1 FS). A unique feature of T2 FS is a footprint of uncertainty (FOU) that is used to characterize additional uncertainties beyond what T1 FS can capture [26, 27]. The membership function of T2 FS is three dimensional and includes a FOU with the new third dimension of T2 FS. A FOU provides additional degrees of freedom that make it possible to provide the capability to model high levels of uncertainties. With these advantages, T2 FLSs have been increasingly applied in engineering fields, such as aircraft maintenance planning, DC–DC converter, hypersonic vehicle, unmanned aerial vehicles, cable-driven parallel system, financial data classification,

wheeled mobile robots, diagnosis of depression, and transport system [25, 28–38]. Type-2 fuzzy logic systems (T2 FLSs) include generalized type-2 fuzzy logic systems (GT2 FLSs) and interval type-2 fuzzy logic system (IT2 FLSs). Considering the simplicity of calculation, this paper adopts an IT2 FLS to model the friction torque.

The steering angular velocity of the front wheels is a necessary factor in the design of the SbW system controller. However, due to the complex mechanical structure and working conditions of the SbW system, the measuring the steering angular velocity is still a difficult problem. Generally, the angular velocity of the front wheels in the SbW system can be obtained in two ways: the angular velocity sensor and numerical methods. First, the angular velocity sensor (gyroscope sensor) can directly measure the angular velocity signal. However, gyroscopes have many disadvantages, such as high price, low signal accuracy due to interference from road conditions, prone to saturation during high rate rotations, and the high failure rate [39]. Besides, the angular velocity sensor increases the installation cost of the system and the complexity of electronic circuits. Considering the hardware cost, the instability of the sensor measurement accuracy, and the sophisticated electronic circuits, the installation of the angular velocity sensor is not the optimal scheme to obtain the steering angular velocity of front wheels. Second, numerical methods, including differentiator and observer, are usually used to obtain the angular velocity of the front wheels. The differentiators/observers designed in [40–43] for mechanical systems require the system to have a bounded-input-bounded-state property, and the angular velocity satisfies the Lipschitz condition. To solve this problem, we designed an observer to estimate the angular velocity of the front wheels in this paper.

To solve the problems of difficult measurement of the angular velocity and control accuracy of the SbW system, this paper proposes an observer-based adaptive interval type-2 fuzzy logic system controller for the steering control of the SbW system. The proposed control strategy does not require an accurate model of the friction torque and the angular velocity sensor. The main works and contributions of this article are:

1. An adaptive interval type-2 fuzzy logic system controller is proposed for the SbW system with the unknown nonlinear friction torque. Compared with the existing model-based friction compensation control methods [8–15], the proposed control strategy does not require an accurate model of the friction torque. Because the friction torque has strong nonlinearity and is easily affected by complex road conditions and many unpredictable factors (lubrication, humidity, contact surface temperature, etc.), it is difficult to

obtain an accurate friction model. This paper proposed a mode-free controller based on interval type-2 fuzzy logic system for the SbW system with unknown friction torque. The adaptive updating laws constructed by estimated error and tracking error can adjust the consequent parameters of IT2 FLS. Finally, the tracking error can be guaranteed to converge asymptotically to zero by the Lyapunov stability theory.

2. Compared with the existing friction modeling methods based on T1 FLS [21–24], the proposed friction modeling method based on IT2 FLS has a more satisfactory effect. The fuzzy sets in T1 FLS are type-1 fuzzy sets, which have accurate membership functions. The accurate membership functions have limitations in dealing with the unknown friction with strong uncertainty. The advantage of the proposed model scheme is that the T2 FS of rule antecedents themselves has the adaptability and novelty. The membership functions of a T2 FS are three dimensional, and it is possible to provide the capability to model high levels of uncertainties. In addition, the consequents parameters of fuzzy rules are derived by the Lyapunov theorem such that adaptive updating laws can effectively adjust the consequent parameters of IT2 FLS. Therefore, this paper uses interval type-2 fuzzy logic system to model the friction torque.
3. Compared with the existing studies for the SbW system [2, 3, 41, 44], the proposed observer-based adaptive interval type-2 fuzzy logic system controller has the following two advantages: ① Different from the existing studies for the SbW system [2, 3, 44], the proposed control strategy does not require an accurate friction torque of the SbW system. ② Different from the existing studies for the SbW system [41], the introduced observer technique no longer requires the assumptions that the bounded-input-bounded-state property of the system and the angular velocity satisfies the Lipschitz condition.
4. The numerical simulations and hardware-in-loop (HIL) experiments verify the effectiveness and superiority of the designed friction compensation control.

The rest of the paper is organized as follows: In Sect. 2, the SbW system and problem formulation are briefly described. In Sect. 3, a detailed introduction of type-2 fuzzy logic system and friction modeling is given. In Sect. 4, the suggested controller and observer are proposed. Sections 5 and 6 provide the simulation results and experimental results of the proposed controller. Finally, the conclusions are drawn in Sect. 7.

Notations: Throughout this paper, \mathbb{R}^n represents the n -dimensional Euclidean space. $\mathbb{R}^{m \times n}$ is the set of $m \times n$ matrices. For a matrix $A \in \mathbb{R}^{n \times m}$, the transpose of A is

defined as $A^T \in \mathbb{R}^{m \times n}$. $|\cdot|$ refers to the absolute value, $\|\cdot\|$ denotes the standard Euclidean vector norm, and $\text{sign}(\cdot)$ is the standard signum function.

2 Dynamics model and problem formulation

The structure of the SbW system is shown in Fig. 1. Different from the traditional steering system, the mechanical link connecting the steering wheel and the front wheels is replaced by a steering motor in the SbW system. The steering motor can drive the front wheels to track the reference signal accurately. The SbW system is mainly composed of the steering motor, driver, reducer, gear box, etc.

2.1 Dynamics model of SbW system

According to the research [45], the dynamic equation of the steering motor assembly module is:

$$J_{sm}\ddot{\delta}_{sm} + B_{sm}\dot{\delta}_{sm} + \tau_{12} = \tau_{sm} \tag{1}$$

The dynamic equation of the front wheels steering model can be modeled as:

$$J_f\ddot{\delta}_f + \tau_{fric} + \tau_e = \tau_f \tag{2}$$

where τ_{fric} is the friction torque of the front wheels, which is discussed in the next subsection. The self-aligning torque τ_e is:

$$\tau_e = \eta \tanh(\delta_f) \tag{3}$$

where η is a positive coefficient that reflects the road conditions. Moreover, the transmission ratio between the steering motor assembly and the front wheels is

$$\frac{\ddot{\delta}_{sm}}{\ddot{\delta}_f} = \frac{\dot{\delta}_{sm}}{\dot{\delta}_f} = \frac{\delta_{sm}}{\delta_f} = \frac{\tau_f}{\tau_{12}} = k \tag{4}$$

which together with Eqs. (1)–(2) gets

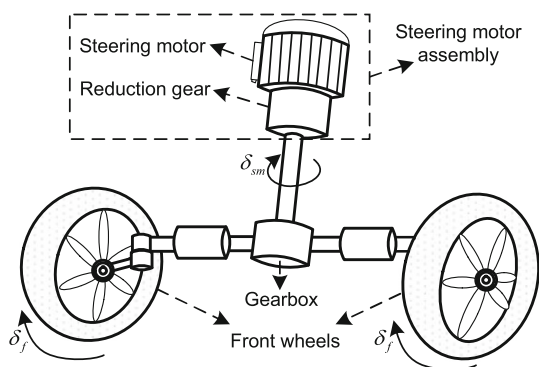


Fig. 1 Dynamics diagram of SbW system

$$J_e\ddot{\delta}_f + B_e\dot{\delta}_f + \tau_{fric} + \tau_e = k\tau_{sm} \tag{5}$$

where $J_e = J_f + k^2J_{sm}$, $B_e = k^2B_{sm}$.

2.2 Friction model

To obtain high steering accuracy, the influence of the friction torque on the SbW system should be fully considered by establishing an accurate friction model. The LuGre model is modeled based on the average deformation of the bristles. The microscopic contact surface can be seen as a large number of elastic bristles with random behavior, and the stiffness of the material on the lower surface is bigger than that on the upper surface (see Fig. 2). The LuGre model with a mathematical expression of first-order differential equation can describe the friction phenomena such as Coulomb friction, viscous friction, Stribeck friction, varying static friction, friction lag, and presliding displacement. The formulation of the LuGre model is

$$\begin{cases} \tau_{fric} = \sigma_0 z + \sigma_1 \dot{z} + \sigma_2 \ddot{\delta}_f \\ \dot{z} = \dot{\delta}_f - |\dot{\delta}_f| \frac{z}{g(\dot{\delta}_f)} \\ \sigma_0 g(\dot{\delta}_f) = F_c + (F_s - F_c) e^{-|\frac{\dot{\delta}_f}{v_s}|^2} \end{cases} \tag{6}$$

where z is the average deflection of the bristles, F_c is the normalized Coulomb friction torque, F_s is the normalized static friction torque, v_s is called the Stribeck velocity, σ_0 , σ_1 , and σ_2 are the hysteresis friction torque parameters that can be physically explained as the stiffness of bristles, damping coefficient, and viscous coefficient, $g(\dot{\delta}_f)$ is used to describe the Stribeck effect.

2.3 Control objective

It is noteworthy that the LuGre friction model can provide an accurate description of the friction phenomenon, although it increases the nonlinearity of the system. Because of the strong nonlinearity of the friction, the complex road conditions, and many unpredictable factors, the unknown parameters of the friction model are difficult to be identified for the practical applications. It is of

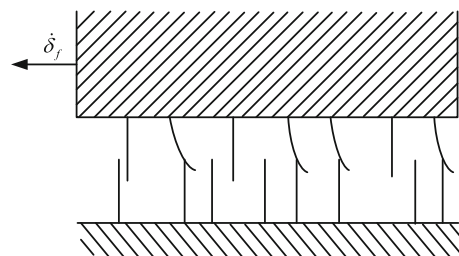


Fig. 2 LuGre friction model

practical significance to use intelligent control method to address the control problem of the SbW system with unknown friction model. The main purpose of this paper is to propose an adaptive interval type-2 fuzzy logic system control for the SbW system, such that the front wheels' steering angle can accurately track its reference signal.

3 Type-2 fuzzy logic system and friction modeling

A detailed introduction of type-2 fuzzy logic system is presented in this section, which includes the basic theory of type-2 fuzzy set and the calculation process of type-2 fuzzy logic system. Then, the friction modeling method based on type-2 fuzzy logic system is designed for the SbW system.

3.1 Type-2 fuzzy set

The membership function of T1 FS is a certain value, which is limited in dealing with the uncertainty. T2 FS fuzzifies the membership function of T1 FS again to improve the fuzziness of fuzzy set. The membership function of T2 FS is three dimensional (see Fig. 3), thus T2 FS has stronger ability to deal with uncertainty and has been widely used in various fields [46–49].

Definition 1 A T2 FS, denoted \tilde{A} , is characterized by a type-2 membership function $\mu_{\tilde{A}}(x, u)$, i.e.,

$$\tilde{A} = \{((x, u), \mu_{\tilde{A}}(x, u)) | x \in X, u \in J_x \subseteq [0, 1]\} \tag{7}$$

where $x \in X$ is the primary variable, $X \subset \mathbb{R}$ is the domain of x , $u \in J_x \subseteq [0, 1]$ is the secondary variable, J_x is called

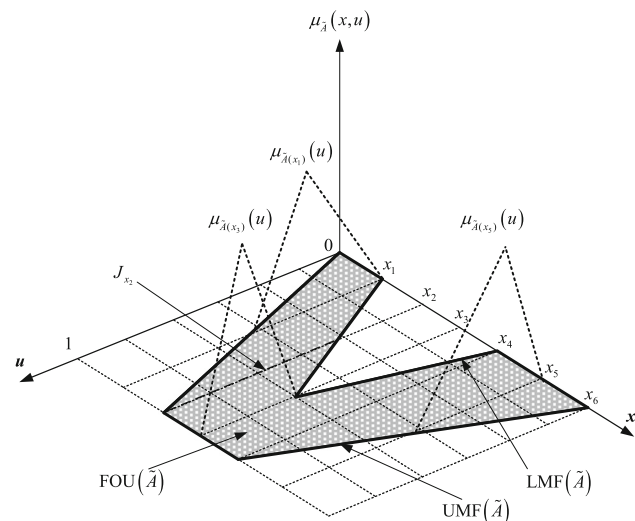


Fig. 3 Various elements of type-2 fuzzy set \tilde{A}

the primary membership of x , $\mu_{\tilde{A}}(x, u)$ is a T1 FS known as the secondary membership. \tilde{A} can also be expressed as

$$\tilde{A} = \int_{x \in X} \int_{u \in J_x} \mu_{\tilde{A}}(x, u) / (x, u) \quad J_x \subseteq [0, 1] \tag{8}$$

where \int denotes union over all admissible x and u .

The 2-D support of $\mu_{\tilde{A}}(x, u)$ is called the FOU of \tilde{A} , i.e., $\text{FOU}(\tilde{A}) = \bigcup_{x \in X} J_x = \{(x, u) \in X \times [0, 1] | \mu_{\tilde{A}}(x, u) > 0\}$. (9)

The upper membership function (UMF) and lower membership function (LMF) of \tilde{A} are two type-1 fuzzy sets that bound the FOU, which are denoted as $\bar{\mu}_{\tilde{A}}(x, u)$ and $\underline{\mu}_{\tilde{A}}(x, u)$, respectively, where

$$\begin{cases} \text{UMF}(\tilde{A}) = \bar{\mu}_{\tilde{A}}(x, u) = \sup\{u | u \in [0, 1], \mu_{\tilde{A}}(x, u) > 0\} \\ \text{LMF}(\tilde{A}) = \underline{\mu}_{\tilde{A}}(x, u) = \inf\{u | u \in [0, 1], \mu_{\tilde{A}}(x, u) > 0\} \end{cases} \tag{10}$$

Definition 2 When all $\mu_{\tilde{A}}(x, u) = 1$, then \tilde{A} is an IT2 FS, i.e.,

$$\tilde{A} = \int_{x \in X} \int_{u \in J_x} 1 / (x, u) \quad J_x \subseteq [0, 1] \tag{11}$$

IT2 FS not only provides the capability to model high levels of uncertainties but also has low computational load, such that it is widely used in engineering practice.

3.2 Type-2 fuzzy logic system

T2 FLSs are usually divided into IT2 FLSs and GT2 FLSs in the literature works. IT2 FLSs, which are the fuzzy logic systems that use at least one IT2 FS, greatly simplified the computational complexity compared with GT2 FLSs, so IT2 FLSs are widely used in engineering practice. IT2 FLSs are applied in this paper for the friction modeling of the SbW system. Due to the simplicity of the calculation, this article focuses on zero-order interval type-2 Takagi-Sugeno-Kang fuzzy logic system (IT2-TSK-FLS), where antecedents are interval type-2 fuzzy sets (IT2 FSs) and consequents are crisp numbers, the j -th rule is the following form:

$$\begin{aligned} R^{(j)} : & \text{IF } x_1 \text{ is } \tilde{A}_1^j, \dots, x_n \text{ is } \tilde{A}_n^j, \\ & \text{THEN } y \text{ is } Y^j \quad j = 1, 2, \dots, M. \end{aligned} \tag{12}$$

where $\tilde{A}_i^j (i = 1, \dots, n)$ are IT2 FSs, b^j are crisp numbers, M is the number of the rules. The detailed calculation process (see Fig. 4) of each module is as follows:

(1) We employ singleton fuzzifier to simplify computation. The result of the input and antecedent operations in

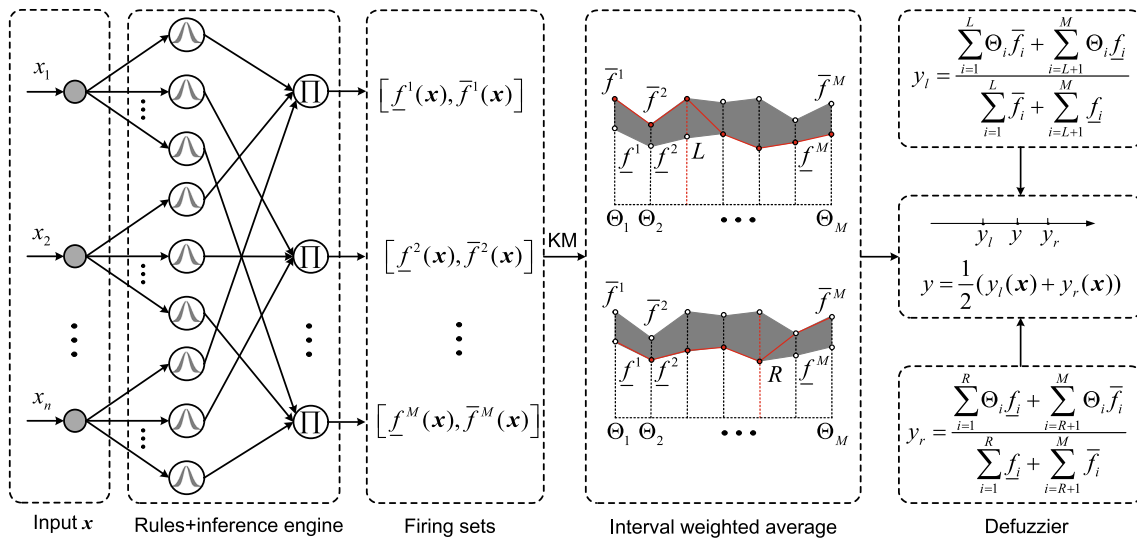


Fig. 4 Calculation process of IT2-TSK-FLS

a rule constitute the firing set. For an input vector $\mathbf{x} = (x_1, \dots, x_n)$, the firing set of each rule is computed as follows:

$$A^j : \begin{cases} F^j(\mathbf{x}) = [f^j(\mathbf{x}), \bar{f}^j(\mathbf{x})] \\ f^j(\mathbf{x}) = \underline{\mu}_{A_1^j}(x_1) \star \dots \star \underline{\mu}_{A_n^j}(x_n) \\ \bar{f}^j(\mathbf{x}) = \bar{\mu}_{A_1^j}(x_1) \star \dots \star \bar{\mu}_{A_n^j}(x_n) \end{cases} \quad (13)$$

where $j = 1, 2, \dots, M$, \star denotes a t-norm, either the minimum or product (we use the product t-norm).

(2) Compute the following interval weighted average:

$$Y_{\text{TSK}}(\mathbf{x}) = 1/[y_l(\mathbf{x}), y_r(\mathbf{x})] \\ = \int_{f^1 \in [f^1, \bar{f}^1]} \dots \int_{f^M \in [f^M, \bar{f}^M]} 1 / \frac{\sum_{j=1}^M f^j b^j}{\sum_{j=1}^M f^j} \quad (14)$$

The interval values $y_l(\mathbf{x})$ and $y_r(\mathbf{x})$ can be calculated by the Karnik–Mendel (KM) algorithm

$$\begin{cases} y_l(\mathbf{x}) = \frac{\sum_{i=1}^L b_i \bar{f}_i + \sum_{i=L+1}^M b_i f_i}{\sum_{i=1}^L \bar{f}_i + \sum_{i=L+1}^M f_i} \\ y_r(\mathbf{x}) = \frac{\sum_{i=1}^R b_i f_i + \sum_{i=R+1}^M b_i \bar{f}_i}{\sum_{i=1}^R f_i + \sum_{i=R+1}^M \bar{f}_i} \end{cases} \quad (15)$$

where L and R are switch points, which are determined by the Karnik–Mendel (KM) algorithms.

(3) The interval $[y_l(\mathbf{x}), y_r(\mathbf{x})]$ is defuzzified to provide the output y

$$y = \frac{1}{2} (y_l(\mathbf{x}) + y_r(\mathbf{x})) = \frac{1}{2} \Theta^T (\zeta_l(\mathbf{x}) + \zeta_r(\mathbf{x})) \quad (16)$$

where $\Theta = [\Theta_1, \dots, \Theta_M]^T = [b^1, \dots, b^M]^T$ is parameter vector, $\zeta_l(\mathbf{x})$ and $\zeta_r(\mathbf{x})$ are left regressive vector and right regressive vector, respectively.

$$\begin{cases} \zeta_l(\mathbf{x}) = \left[\frac{\bar{f}_1}{D_l}, \dots, \frac{\bar{f}_L}{D_l}, \frac{f_{L+1}}{D_l}, \dots, \frac{f_M}{D_l} \right]^T \\ \zeta_r(\mathbf{x}) = \left[\frac{f_1}{D_r}, \dots, \frac{f_L}{D_r}, \frac{\bar{f}_{R+1}}{D_r}, \dots, \frac{\bar{f}_M}{D_r} \right]^T \end{cases} \quad (17)$$

where $D_l = \sum_{i=1}^L \bar{f}_i + \sum_{i=L+1}^M f_i$ and

$$D_r = \sum_{i=1}^R f_i + \sum_{i=R+1}^M \bar{f}_i.$$

For the ability of zero-order IT2-TSK-FLS to approach a real continuous function on a compact set, we have the following lemma.

Lemma 1 [25] For any continuous function $f(\mathbf{x})$ defined on a compact set Ω_x . Then, there exists a zero-order IT2-TSK-FLS as (16) for any $\delta \geq 0$ such that

$$\sup_{\mathbf{x} \in \Omega_x} |f(\mathbf{x}) - \frac{1}{2} \Theta^T (\zeta_l(\mathbf{x}) + \zeta_r(\mathbf{x}))| < \delta \quad (18)$$

Remark 1 Zero-order IT2-TSK-FLS is selected for friction modeling, in which the consequent parameters of fuzzy rules are updated by adaptive laws derived by the Lyapunov stability theory. The consequent components of fuzzy rules are crisp numbers instead of intervals. Both sides of the intervals represent the left and right end points of the centroid of T2 FSs. Therefore, it is avoided that the left centroid is larger than the right centroid in the adaptive process.

Remark 2 FLS and neural network have a common goal: to imitate the operation mechanism of the human brain. These two models are motivated from different origins (neural networks from physiology and fuzzy logic systems from cognitive science). As a common neural network structure, radial basis function network (RBFN) is proposed by Moody and Darken [50] based on the biological receptive fields. Fuzzy logic systems are composed of fuzzy concepts and fuzzy logic. It captures the fuzziness of human brain thinking and imitates human comprehensive inference to deal with fuzzy information processing problems that are difficult to solve by conventional mathematical methods. Fuzzy logic system and RBFN share common characteristics not only in their operations on data, but also in data-driven nonlinear system modeling as the universal approximator [51–54]. Type-2 fuzzy set is an extension of the concept of the traditional type-1 fuzzy set, and its membership function is three dimensional. Because of the characteristics of type-2 fuzzy set, Interval type-2 fuzzy logic system has a stronger ability to deal with uncertainty than the traditional fuzzy logic system.

3.3 Friction modeling

For brevity, the dynamics model of the SbW system (5) can be rewritten as

$$\begin{cases} \dot{\delta} = A\delta + B(\tau_{\Delta fric} + g\tau_{sm}) \\ y = C^T\delta \end{cases} \quad (19)$$

where state vector $\delta = [\delta_f, \dot{\delta}_f]^T \in \mathbb{R}^2$, $g = k/J_e$, $A = [0, 1; 0, 0]^T$, $B = [0, 1]^T$, $C = [1, 0]^T$, the lumped friction torque $\tau_{\Delta fric} = -\frac{1}{J_e}(\tau_{fric} + \tau_e + B_e\dot{\delta}_f)$.

Through the previous analysis, $\tau_{\Delta fric}$ is related to the steering angle δ_f and the angular velocity $\dot{\delta}_f$. Because the desired steering angle δ_d and the desired angular velocity $\dot{\delta}_d$ are known, $\tau_{\Delta fric}$ can be regarded as a function of the steering angle error e and the steering angle velocity error \dot{e} . Therefore, the real continuous function $\tau_{\Delta fric}$ in Eq. (19) is approximated by zero-order IT2-TSK-FLS in the following form:

$$\tau_{\Delta fric} = \frac{1}{2}\Theta^{*T}(\zeta_l(e) + \zeta_r(e)) + \omega_{\Delta fric} \quad (20)$$

where $e = [e, \dot{e}]^T \in \mathbb{R}^2$, $e = \delta_f - \delta_d$, $\omega_{\Delta fric}$ is the minimal approximation errors, Θ^* is the optimal parameter, which are defined as:

$$\Theta^* = \arg \min_{\Theta \in \Omega_\Theta} [\sup_{e \in \Omega_e} \|\hat{\tau}_{\Delta fric}(e|\Theta) - \tau_{\Delta fric}\|] \quad (21)$$

where $\Omega_\Theta = \{\Theta | \|\Theta\| \leq M\}$, $\Omega_e = \{e | \|e\| \leq M_e\}$, $\hat{\tau}_{\Delta fric}(e|\Theta) = \frac{1}{2}\Theta^T(\zeta_l(e) + \zeta_r(e))$, M and M_e are positive scalar value.

4 Observer-based adaptive fuzzy control

There are three parts in this section. Firstly, the front wheels' angular velocity is obtained by an observer instead of the angular velocity sensor. Secondly, an observer-based adaptive interval type-2 fuzzy logic system controller is designed to ensure the steering performance of the SbW system with the nonlinear friction torque. The designed controller need not the prior knowledge about the nonlinear friction torque. Finally, the Lyapunov stability theory is used to analyze the stability of the control system.

4.1 Observer design

In the practical application, the installation of the angular velocity sensor will improve the structural complexity and hardware cost and reduce the system reliability. In this paper, the following observer that estimates the state error e is designed as [55]

$$\begin{cases} \dot{\hat{e}} = A\hat{e} - BK_c^T\hat{e} + K_0C^T\tilde{e} \\ \hat{e}_1 = C^T\hat{e} \end{cases} \quad (22)$$

where \hat{e} denotes the estimate of e , $\hat{e} = [\hat{e}, \dot{\hat{e}}]^T \in \mathbb{R}^2$, $\tilde{e} = e - \hat{e}$ is the observation error, K_c is chosen such that the matrix $A - BK_c$ is Hurwitz. Thus, there exist symmetric positive definite matrices P_1 and Q_1 such that

$$(A - BK_c^T)^TP_1 + P_1(A - BK_c^T) = -Q_1 \quad (23)$$

Estimate error \hat{e} replaces e as input variables of IT2 FLS (20), then we can have the approximate value of $\tau_{\Delta fric}$ as:

$$\hat{\tau}_{\Delta fric}(\hat{e}|\Theta) = \frac{1}{2}\Theta^T(\zeta_l(\hat{e}) + \zeta_r(\hat{e})) \quad (24)$$

4.2 Robust controller design

Based on the above IT2 FLS (24) and the designed error observer (22), the controller is designed for the SbW system as follows:

$$\tau_{sm} = \tau_c + \tau_r \quad (25)$$

$$\tau_c = \frac{1}{g}(\ddot{\delta}_d - K_c^T\hat{e} - \hat{\tau}_{\Delta fric}(\hat{e}|\Theta)) \quad (26)$$

Substituting Eq. (25) into Eq. (19), we can obtain the dynamic equation

$$\begin{cases} \dot{\delta} = A\delta + B(\tau_{\Delta fric} + g\tau_c + g\tau_r) \\ y = C^T\delta \end{cases} \tag{27}$$

Then, the tracking error dynamic equation be derived as:

$$\begin{cases} \dot{e} = Ae + B[(\tau_{\Delta fric} - \hat{\tau}_{\Delta fric}(\hat{e}|\Theta)) + g\tau_r - K_c^T\hat{e}] \\ e_1 = C^Te \end{cases} \tag{28}$$

Subtracting Eq. (22) from Eq. (28) yields

$$\begin{cases} \dot{\tilde{e}} = (A - K_0C^T)\tilde{e} + B[(\tau_{\Delta fric} - \hat{\tau}_{\Delta fric}(\hat{e}|\Theta)) + g\tau_r] \\ \tilde{y} = C^T\tilde{e} \end{cases} \tag{29}$$

Equation (29) can be written as

$$\tilde{y} = H(s)[(\tau_{\Delta fric} - \hat{\tau}_{\Delta fric}(\hat{e}|\Theta)) + g\tau_r] \tag{30}$$

where the transfer function $H(s) = C^T(sI - (A - K_0C^T))^{-1}B$ of Eqs. (29) and (30) is known stable. Since only \tilde{y} is measurable, in order to use the strict positive real (SPR)-Lyapunov synthesis approach, Eq. (30) can be rewritten as $\tilde{y} = H(s)L(s)L^{-1}(s)[(\tau_{\Delta fric} - \hat{\tau}_{\Delta fric}(\hat{e}|\Theta)) + g\tau_r]$ (31)

where $L(s) = s^m + b_1s^{m-1} + \dots + b_m$ is appropriately selected so that $H(s)L(s)$ is SPR transfer function [56]. Eq.(31) can be expressed as follows:

$$\begin{cases} \dot{\tilde{e}} = (A - K_0C^T)\tilde{e} + B_cL^{-1}(s)[(\tau_{\Delta fric} - \hat{\tau}_{\Delta fric}(\hat{e}|\Theta)) \\ + g\tau_r] \\ \tilde{y} = C^T\tilde{e} \end{cases} \tag{32}$$

Since $H(s)L(s)$ is a proper SPR transfer function, according to the Kalman–Yakubovich lemma [58], it can be seen that there are positive definite matrices P_2 and Q_2 such that:

$$\begin{cases} (A - K_0C^T)^T P_2 + P_2(A - K_0C^T) = -Q_2 \\ P_2 B_c = C \end{cases} \tag{33}$$

Equation (32) can be rewritten as

$$\begin{cases} \dot{\tilde{e}} = (A - K_0C^T)\tilde{e} + B_c \left(\left[\frac{1}{2}\tilde{\Theta}^T(\xi_l(\hat{e}) + \xi_r(\hat{e})) + \omega \right] \right. \\ \left. + B_cL^{-1}(s)g\tau_r \right) \\ \tilde{y} = C^T\tilde{e} \end{cases} \tag{34}$$

where $\tilde{\Theta} = \Theta^* - \Theta$, $\omega = -\frac{1}{2}\tilde{\Theta}^T(\xi_l(\hat{e}) + \xi_r(\hat{e})) + L^{-1}(s)\frac{1}{2}$

$$\begin{aligned} & \tilde{\Theta}^T(\xi_l(\hat{e}) + \xi_r(\hat{e})) + \frac{1}{2}\Theta^{*T}((\xi_l(e) + \xi_r(e)) \\ & - (\xi_l(\hat{e}) + \xi_r(\hat{e}))) + \omega_{\Delta fric} \end{aligned}$$

, ω is a lumped modeling error, and there is an unknown upper bound ϖ , $|\omega| \leq \varpi$.

4.3 Stability analysis

Theorem 1 For the SBW system described in Eq. (19), the observer is designed as Eq. (22), the adaptive fuzzy controller is formulated as Eq. (25), the robust term τ_r which includes Nussbaum-type function is designed as

$$\tau_r = \left(\frac{\tilde{y}\hat{\omega}^2}{\hat{\omega}|\tilde{y}| + \sigma^2} + K_o^T P_1 \hat{e} \right) N(\zeta) \tag{35}$$

$$\dot{\zeta} = \frac{\tilde{y}^2\hat{\omega}^2}{\hat{\omega}|\tilde{y}| + \sigma^2} + \tilde{y}K_o^T P_1 \hat{e} \tag{36}$$

where $N(\zeta) = \exp(\zeta^2) \cos((\pi/2)\zeta)$, $\hat{\omega}$ is the estimate of ω , σ is a varying parameter designed later. The update laws are selected to adjust the unknown parameters Θ , ϖ and σ :

$$\dot{\Theta} = \begin{cases} \frac{1}{2}\gamma_1\tilde{y}[\xi_l(\hat{e}) + \xi_r(\hat{e})], & \text{if } \|\Theta\| < M \text{ or } (\|\Theta\| = M \\ & \text{and } [\xi_l(\hat{e}) + \xi_r(\hat{e})]^T\Theta\tilde{y} \leq 0) \\ P[\cdot], & \text{if } \|\Theta\| = M \\ & \text{and } [pmb\xi_l(\hat{e}) + \xi_r(\hat{e})]^T\Theta\tilde{y} > 0 \end{cases} \tag{37}$$

$$\dot{\hat{\omega}} = \gamma_2|\tilde{y}| \tag{38}$$

$$\dot{\sigma} = -\gamma_3\sigma \tag{39}$$

where γ_1 , γ_2 , and γ_3 are given constants, $P[\cdot]$ projection operator can be expressed as

$$P[\cdot] = \frac{1}{2}\gamma_1\tilde{y}[\xi_l(\hat{e}) + \xi_r(\hat{e})] - \frac{1}{2}\gamma_1 \frac{\tilde{y}[\xi_l(\hat{e}) + \xi_r(\hat{e})]^T\Theta}{\|\Theta\|^2}\Theta \tag{40}$$

Then, the tracking error e can converge asymptotically to zero. Fig. 5 describes the control process of the SbW system.

Nussbaum-type function is used in Eq. (35). The relevant definition and lemma are as follows:

Definition 2 The function $N(\zeta)$ is called Nussbaum gain function if the following properties are held:

$$\limsup_{s \rightarrow \infty} \frac{1}{s} \int_0^s N(\zeta)d\zeta = +\infty \tag{41}$$

$$\liminf_{s \rightarrow \infty} \frac{1}{s} \int_0^s N(\zeta)d\zeta = -\infty \tag{42}$$

Nussbaum functions commonly used in the literature are $\zeta^2 \cos(\zeta)$, $\zeta^2 \sin(\zeta)$, and $\exp(\zeta^2) \cos((\pi/2)\zeta)$. In this paper, $\exp(\zeta^2) \cos((\pi/2)\zeta)$ is used as a Nussbaum function.

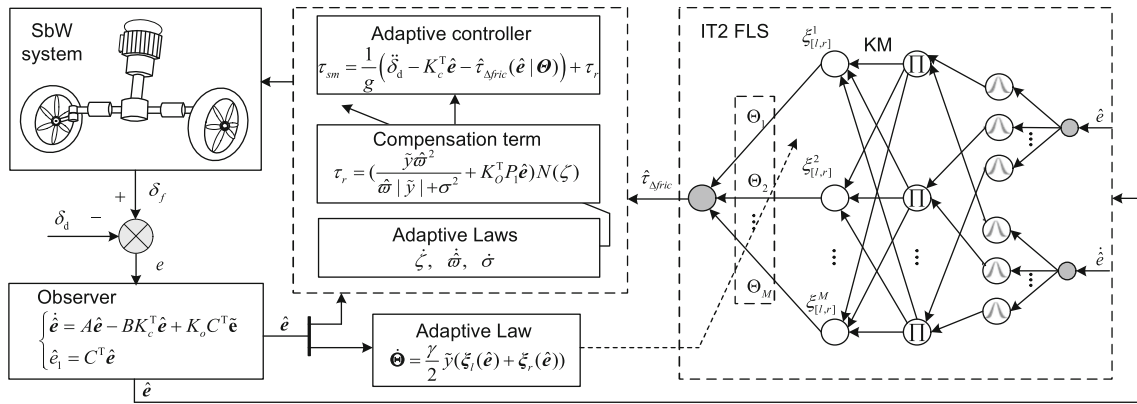


Fig. 5 Principle control diagram

Lemma 2 [56, 57] Let $V(t)$ and $\zeta(t)$ to be a smooth function on interval $[0, t_f)$, with $V > 0, \forall t \in [0, t_f)$, and $N(\zeta)$ is an even smooth Nussbaum-type function. If the following inequality is satisfied:

$$V(t) \leq c_0 + \int_0^t (g(v)N(\zeta(v)) + 1)\dot{\zeta}(v)dv, \forall t \in [0, t_f) \tag{43}$$

where c_0 represents some suitable constant, and $g(v)$ is a nonzero time-varying function, then $V(t), \zeta(t)$ and $\int_0^t (g(v)N(\zeta(v)) + 1)\dot{\zeta}(v)dv$ must be bounded on $t \in [0, t_f)$.

Proof we consider Lyapunov function:

$$V = \frac{1}{2}\hat{e}^T P_1 \hat{e} + \frac{1}{2}\tilde{e}^T P_2 \tilde{e} + \frac{1}{2\gamma_1} \tilde{\Theta}^T \tilde{\Theta} + \frac{1}{2\gamma_2} \tilde{\omega}^2 + \frac{1}{2\gamma_3} \sigma^2 \tag{44}$$

Differentiating (44) with respect to time yields

$$\dot{V} = \frac{1}{2}\dot{\hat{e}}^T P_1 \hat{e} + \frac{1}{2}\hat{e}^T P_1 \dot{\hat{e}} + \frac{1}{2}\dot{\tilde{e}}^T P_2 \tilde{e} + \frac{1}{2}\tilde{e}^T P_2 \dot{\tilde{e}} + \frac{1}{\gamma_1} \tilde{\Theta}^T \dot{\tilde{\Theta}} + \frac{1}{\gamma_2} \tilde{\omega} \dot{\tilde{\omega}} + \frac{1}{\gamma_3} \sigma \dot{\sigma} \tag{45}$$

From Eq. (22) and Eq. (34), we have

$$\begin{aligned} \dot{V} = & \frac{1}{2}[\hat{e}^T(A - BK_c^T)^T P_1 \hat{e} + \tilde{e}^T CK_o^T P_1 \tilde{e} + \hat{e}^T P_1 (A - BK_c^T) \hat{e} + \tilde{e}^T P_1 K_0 C^T \tilde{e}] + \frac{1}{2}[\tilde{e}^T (A - K_0 C^T)^T P_2 \tilde{e} \\ & + \frac{1}{2}(\xi_l(\hat{e}) + \xi_r(\hat{e}))^T \tilde{\Theta} B_c^T P_2 \tilde{e} + L^{-1}(s)g\tau_r B_c^T P_2 \tilde{e} \\ & + \omega B_c^T P_2 \tilde{e} + \tilde{e}^T P_2 (A - K_0 C^T) \tilde{e} + \frac{1}{2}\tilde{e}^T P_2 B_c \tilde{\Theta}^T \\ & (\xi_l(\hat{e}) + \xi_r(\hat{e})) + \tilde{e}^T P_2 B_c L^{-1}(s)g\tau_r + \tilde{e}^T P_2 B_c \omega] \\ & + \frac{1}{\gamma_1} \tilde{\Theta}^T \dot{\tilde{\Theta}} + \frac{1}{\gamma_2} \tilde{\omega} \dot{\tilde{\omega}} + \frac{1}{\gamma_3} \sigma \dot{\sigma} \end{aligned} \tag{46}$$

The above equation can be further derived as

$$\begin{aligned} \dot{V} = & -\frac{1}{2}\hat{e}^T ((A - BK_c^T)^T P_1 + P_1 (A - BK_c^T)) \hat{e} \\ & -\frac{1}{2}\tilde{e}^T ((A - K_0 C^T)^T P_2 + P_2 (A - K_0 C^T)) \tilde{e} \\ & + \left[\frac{1}{2}(\xi_l(\hat{e}) + \xi_r(\hat{e}))^T B_c^T P_2 \tilde{e} + \frac{1}{\gamma_1} \tilde{\Theta}^T \dot{\tilde{\Theta}} \right] \\ & + \tilde{e}^T CK_o^T P_1 \tilde{e} + \tilde{e}^T P_2 B_c L^{-1}(s)g\tau_r + \tilde{e}^T P_2 B_c \omega + \frac{1}{\gamma_2} \tilde{\omega} \dot{\tilde{\omega}} + \frac{1}{\gamma_3} \sigma \dot{\sigma} \end{aligned} \tag{47}$$

After further calculation, we can get

$$\dot{V} = -\frac{1}{2}\hat{e}^T Q_1 \hat{e} - \frac{1}{2}\tilde{e}^T Q_2 \tilde{e} + \frac{1}{\gamma_2} \tilde{\omega} \dot{\tilde{\omega}} + \frac{1}{\gamma_3} \sigma \dot{\sigma} + S_\Omega \tag{48}$$

where

$$\begin{aligned} S_\Omega = & \tilde{y}L^{-1}(s)g\tau_r + \tilde{y}^T K_o^T P_1 \hat{e} + \tilde{y}\omega \\ = & \tilde{y}L^{-1}(s)g\tau_r + \tilde{y}g\tau_r - \tilde{y}g\tau_r + \tilde{y}^T K_o^T P_1 \hat{e} + \tilde{y}\omega \\ \leq & \tilde{y}g_1(t)\tau_r + \tilde{y}^T K_o^T P_1 \hat{e} + |\tilde{y}| \varpi \\ \leq & -|\tilde{y}| |\tilde{\omega}| + |\tilde{y}| |\hat{\omega}| + \tilde{y}g_1(t)\tau_r + \tilde{y}^T K_o^T P_1 \hat{e} \\ \leq & -|\tilde{y}| |\tilde{\omega}| + (1 + g_1(t)N(\zeta))\dot{\zeta} + |\tilde{y}| |\hat{\omega}| \\ & - \frac{\tilde{y}^2 \tilde{\omega}^2}{|\tilde{y}| |\hat{\omega}| + \sigma^2} \\ \leq & -|\tilde{y}| |\tilde{\omega}| + (1 + g_1(t)N(\zeta))\dot{\zeta} + \sigma^2 \end{aligned} \tag{49}$$

□

where $\varpi = \hat{\omega} - \tilde{\omega}, g_1(t) = g + [g_2 + g]\text{sign}(\tilde{y}\tau_r), |L^{-1}(s)g| \leq g_2$. Substituting Eq. (49) into Eq. (48), we can get:

$$\begin{aligned} \dot{V}(t) \leq & -\frac{1}{2}\hat{e}^T Q_1 \hat{e} - \frac{1}{2}\tilde{e}^T Q_2 \tilde{e} + (1 + g_1(t)N(\zeta))\dot{\zeta} \\ & + \tilde{\omega} \left(\frac{1}{\gamma_2} \dot{\tilde{\omega}} - |\tilde{y}| \right) + \sigma \left(\frac{1}{\gamma_3} \dot{\sigma} + \sigma \right) \end{aligned} \tag{50}$$

Substituting Eqs. (38)–(39) into above equation, we can get:

$$\dot{V}(t) \leq -\frac{1}{2}\hat{e}^T Q_1 \hat{e} - \frac{1}{2}\tilde{e}^T Q_2 \tilde{e} + (1 + g_1(t)N(\zeta))\dot{\zeta} \quad (51)$$

Considering $e_a = [\hat{e}, \tilde{e}]^T$, $Q = \text{diag}[Q_1, Q_2]$, then we have

$$\begin{aligned} \dot{V} &\leq -\frac{1}{2}e_a^T Q e_a + (1 + g_1(t)N(\zeta))\dot{\zeta} \\ &\leq (1 + g_1(t)N(\zeta))\dot{\zeta} \end{aligned} \quad (52)$$

Integrating the above equation yields

$$V(t) - V(0) \leq \int_0^t (1 + g_1(v)N(\zeta))\dot{\zeta}(v)dv \quad (53)$$

According to Lemma 2, it can be concluded from the above equation that $V(t)$, $V(0)$, and $\int_0^t [1 + g_1(v)]N(\zeta)\dot{\zeta}dv$ are bounded on $[0, t_f]$. The above conclusion also holds when $t_f \rightarrow +\infty$ [56]. We can know that \hat{e} , \tilde{e} , $\hat{\Theta}$, $\tilde{\omega}$ and σ are bounded, so it is further concluded that the control input τ_{sm} is bounded. According to Eq. (52), it can be obtained that:

$$\begin{aligned} \frac{1}{2} \int_0^t e_a^T Q e_a dv &\leq V(0) - V(t) \\ &+ \int_0^t (1 + g_1(v)N(\zeta))\dot{\zeta}(v)dv \end{aligned} \quad (54)$$

This implies that $\hat{e} \in L_2$, $\tilde{e} \in L_2$. According to Eq. (22) and Eq. (34), we can know that $\dot{\hat{e}} \in L_\infty$, $\dot{\tilde{e}} \in L_\infty$. Because $\hat{e} \in L_2 \cap L_\infty$ and $\dot{\hat{e}} \in L_\infty$, $\tilde{e} \in L_2 \cap L_\infty$ and $\dot{\tilde{e}} \in L_\infty$, by using the Barbalat lemma [58, 59], we can get that $\lim_{t \rightarrow \infty} \hat{e} = 0$ and $\lim_{t \rightarrow \infty} \tilde{e} = 0$. Therefore, $\lim_{t \rightarrow \infty} e = 0$. The pseudocode of proposed AIT2FLSC algorithm is shown in Fig. 6.

Remark 3 In engineering practice, the parameter drift problems are usually occurred due to the use of the adaptive laws (36), (38)–(39). In order to avoid the parameter drift problems, the following deadzone technique is employed [60]:

$$\dot{\zeta} = \begin{cases} \frac{\tilde{y}^2 \hat{\omega}^2}{\hat{\omega} |\tilde{y}| + \sigma^2} + \tilde{y} K_o^T P_1 \hat{e}, & \text{if } |e| \geq \varepsilon \\ 0, & \text{if } |e| < \varepsilon \end{cases} \quad (55)$$

$$\dot{\hat{\omega}} = \begin{cases} \gamma_2 |\tilde{y}|, & \text{if } |e| \geq \varepsilon \\ 0, & \text{if } |e| < \varepsilon \end{cases} \quad (56)$$

$$\dot{\sigma} = \begin{cases} -\gamma_3 \sigma, & \text{if } |e| \geq \varepsilon \\ 0, & \text{if } |e| < \varepsilon \\ \text{quadif } |e| < \varepsilon \end{cases} \quad (57)$$

where ε is the dead zone size.

5 Simulation results

In this section, to validate the effectiveness of the proposed adaptive interval type-2 fuzzy logic system controller (AIT2FLSC) for the SbW system with nonlinear friction torque, numerical simulations are carried out in two different friction environments. In addition, we use the adaptive type-1 fuzzy logic system controller (AT1F LSC) to verify the advantages of proposed controller from different aspects.

Step 1: Set SBW system parameters

The self-aligning torque τ_e can be regarded as $\tau_e = 950 \tanh(\delta_f)$. The nominal parameters of the SbW system in Eq. (19) are chosen as follows: $J_f = 3.8 \text{ kg}\cdot\text{m}^2$, $k = 18$, $B_{sm} = 0.05 \text{ Nms/rad}$, $J_{sm} = 0.0045 \text{ kg}\cdot\text{m}^2$, $\sigma_0 = 39000$, $\sigma_1 = 780$, $\sigma_2 = 30$, $v_s = 0.03$.

To verify the effectiveness and adaptability of the proposed control method, the parameters and structures of the friction model in simulations are assumed to change gradually as shown in Table 1. The Luge friction model is used in Environment 1. The structure of the friction model does not change during the simulation, but the parameters change. The Coulomb friction model, the Stribeck friction model and the Luge friction model are used in Environment 2. The model structures and parameters change simultaneously.

Step 2: Establish IT2 FLS system

The input variables of IT2 FLS are selected as \hat{e} and $\dot{\hat{e}}$. Set the fuzzy rules of IT2 FLS as follows:

$$\begin{aligned} R^{(j)} : & \text{IF } \hat{e} \text{ is } \tilde{A}_1^j, \dot{\hat{e}} \text{ is } \tilde{A}_2^j, \\ & \text{THEN } \tau_{\Delta\text{fric}} \text{ is } b^j \quad j = 1, 2, \dots, 5. \end{aligned} \quad (58)$$

where $\tilde{A}_1^j = \tilde{A}_2^j$ are IT2 FSs of the input variables. Then, the membership functions are chosen as follows:

$$\begin{aligned} \bar{\mu}_{A_1^1}(\hat{e}) &= 1/(1 + \exp((72 \times (\hat{e} + 0.02))))), \\ \underline{\mu}_{A_1^1}(\hat{e}) &= 1/(1 + \exp((70 \times (\hat{e} + 0.05))))); \\ \bar{\mu}_{A_1^2}(\hat{e}) &= \exp(-(500 \times (\hat{e} + 0.02)^2)), \\ \underline{\mu}_{A_1^2}(\hat{e}) &= \exp(-(1100 \times (\hat{e} + 0.02)^2)); \\ \bar{\mu}_{A_1^3}(\hat{e}) &= \exp(-(500 \times \hat{e}^2)), \underline{\mu}_{A_1^3}(\hat{e}) = \exp(-(1100 \times \hat{e}^2)); \\ \bar{\mu}_{A_1^4}(\hat{e}) &= \exp(-(500 \times (\hat{e} - 0.02)^2)), \\ \underline{\mu}_{A_1^4}(\hat{e}) &= \exp(-(1100 \times (\hat{e} - 0.02)^2)); \end{aligned}$$

$$\begin{aligned} \bar{\mu}_{A_1^5}(\hat{e}) &= 1/(1 + \exp((-72 \times (\hat{e} - 0.02))))), \underline{\mu}_{A_1^5}(\hat{e}) \\ &= 1/(1 + \exp((-70 \times (\hat{e} - 0.05)))). \end{aligned}$$

AIT2FLSC algorithm

Selections of initial parameters:

Select the initial parameters of the SbW systems $\delta(0)=0$; the initial parameters of the observer $\hat{e}(0) = 0$; the initial values of adaptive parameters $\Theta(0) = [-420, -280, 0, 280, 420]$, $\zeta(0) = 0$ and $\sigma(0) = 0.001$.

Selections of observer parameters:

- ① Select K_c and K_0 such that the matrices $A - BK_c$ and $A - K_0C^T$ are Hurwitz, respectively.
- ② Select symmetric positive definite matrices P_1 and Q_1 such that $(A - BK_c^T)^T P_1 + P_1(A - BK_c^T) = -Q_1$.
- ③ Select appropriate $L(s)$ so that $H(s)L(s)$ is SPR transfer function.
- ④ Select the asymmetric positive definite matrices P_2 and Q_2 such that:
 $(A - K_0C^T)^T P_2 + P_2(A - K_0C^T) = -Q_2, P_2 B_c = C$.

Establish interval type-2 fuzzy logic system:

Choose the number of fuzzy rules M and membership functions $\underline{\mu}_{\tilde{A}_1^j}(\hat{e}), \bar{\mu}_{\tilde{A}_1^j}(\hat{e}), \underline{\mu}_{\tilde{A}_2^j}(\hat{e})$ and $\bar{\mu}_{\tilde{A}_2^j}(\hat{e})$.

Selections of controller parameters:

Choose the values $\gamma_1 > 0, \gamma_2 > 0, \gamma_3 > 0, \varepsilon > 0$ in (37)-(39), (55)-(57).

Calculation process:

Step 1: Solve the following observer to obtain the estimated value \hat{e} .

$$\begin{cases} \dot{\hat{e}} = A\hat{e} - BK_c^T \hat{e} + K_0 C^T \tilde{e} \\ \hat{e}_1 = C^T \hat{e} \end{cases}$$

Step 2: For the fuzzy rules (58) of IT2 FLS, the firing set of each rule is computed as follows:

$$\tilde{A}^j : \begin{cases} F^j(\hat{e}) = [\underline{f}^j(\hat{e}), \bar{f}^j(\hat{e})] \\ \underline{f}^j(\hat{e}) = \underline{\mu}_{\tilde{A}_1^j}(\hat{e}) * \underline{\mu}_{\tilde{A}_2^j}(\hat{e}) \\ \bar{f}^j(\hat{e}) = \bar{\mu}_{\tilde{A}_1^j}(\hat{e}) * \bar{\mu}_{\tilde{A}_2^j}(\hat{e}) \end{cases}$$

Step 3: Compute the following interval weighted average:

$$Y_{\text{TSK}}(\hat{e}) = 1/[y_l(\hat{e}), y_r(\hat{e})] = \int_{f^1 \in [\underline{f}^1, \bar{f}^1]} \cdots \int_{f^M \in [\underline{f}^M, \bar{f}^M]} 1 / \frac{\sum_{j=1}^M f^j b^j}{\sum_{j=1}^M f^j}$$

The interval values $y_l(\hat{e})$ and $y_r(\hat{e})$ can be calculated by the KM algorithm

$$\begin{cases} y_l(\hat{e}) = \frac{\sum_{i=1}^L b_i \bar{f}_i + \sum_{i=L+1}^M b_i \underline{f}_i}{\sum_{i=1}^L \bar{f}_i + \sum_{i=L+1}^M \underline{f}_i}, \\ y_r(\hat{e}) = \frac{\sum_{i=1}^R b_i \underline{f}_i + \sum_{i=R+1}^M b_i \bar{f}_i}{\sum_{i=1}^R \underline{f}_i + \sum_{i=R+1}^M \bar{f}_i}. \end{cases}$$

where L and R are switch points, which are determined by the KM algorithm.

Step 4: Compute the fuzzy basis functions $\xi_l(\hat{e})$ and $\xi_r(\hat{e})$:

$$\begin{cases} \xi_l(\hat{e}) = \left[\frac{\bar{f}_1}{D_l}, \dots, \frac{\bar{f}_L}{D_l}, \frac{\underline{f}_{L+1}}{D_l}, \dots, \frac{\underline{f}_M}{D_l} \right]^T \\ \xi_r(\hat{e}) = \left[\frac{\underline{f}_1}{D_r}, \dots, \frac{\underline{f}_R}{D_r}, \frac{\bar{f}_{R+1}}{D_r}, \dots, \frac{\bar{f}_M}{D_r} \right]^T \end{cases}$$

where $D_l = \sum_{i=1}^L \bar{f}_i + \sum_{i=L+1}^M \underline{f}_i$ and $D_r = \sum_{i=1}^R \underline{f}_i + \sum_{i=R+1}^M \bar{f}_i$.

Step 5: Compute the update laws:

$$\begin{cases} \dot{\zeta} = \frac{\tilde{y}^2 \hat{\omega}^2}{\hat{\omega}|\tilde{y}| + \sigma^2} + \tilde{y} K_o^T P_1 \hat{e} \\ \dot{\Theta} = \begin{cases} \frac{1}{2} \gamma_1 \tilde{y} [\xi_l(\hat{e}) + \xi_r(\hat{e})], & \text{if } \|\Theta\| < M \text{ or } (\|\Theta\| = M \\ & \text{and } [\xi_l(\hat{e}) + \xi_r(\hat{e})]^T \Theta \tilde{y} \leq 0) \\ P[\cdot], & \text{if } \|\Theta\| = M \\ & \text{and } [\xi_l(\hat{e}) + \xi_r(\hat{e})]^T \Theta \tilde{y} > 0 \end{cases} \\ \dot{\hat{\omega}} = \gamma_2 |\tilde{y}| \\ \dot{\sigma} = -\gamma_3 \sigma \end{cases}$$

Step 6: Compute the controller:

$$\begin{cases} \tau_{sm} = \tau_c + \tau_r \\ \tau_c = \frac{1}{g} (\delta_d - K_c^T \hat{e} - \hat{\tau}_{\Delta \text{fric}}(\hat{e}|\Theta)) \\ \tau_r = \left(\frac{\tilde{y} \hat{\omega}^2}{\hat{\omega}|\tilde{y}| + \sigma^2} + K_o^T P_1 \hat{e} \right) N(\zeta) \end{cases}$$

Step 7: Apply controller to the SbW systems, then the SbW systems generates new state variables δ_f and return **Step 1**.

Fig. 6 The pseudocode of proposed AIT2FLSC algorithm

Table 1 Friction model parameters and structures

Environment	Friction model $\tau_{fric}(t/s)$					
	$t \in [0, 30]s$	$t \in (30, 60]s$	$t \in (60, 90]s$	$t \in (90, 120]s$	$t \in (120, 150]s$	$t \in (150, 180]s$
Environment 1	Lugre	Lugre	Lugre	Lugre	Lugre	Lugre
	$F_c = 25 \text{ Nm}$ $F_s = 30 \text{ Nm}$	$F_c = 30 \text{ Nm}$ $F_s = 35 \text{ Nm}$	$F_c = 35 \text{ Nm}$ $F_s = 40 \text{ Nm}$	$F_c = 40 \text{ Nm}$ $F_s = 45 \text{ Nm}$	$F_c = 45 \text{ Nm}$ $F_s = 50 \text{ Nm}$	$F_c = 38 \text{ Nm}$ $F_s = 43 \text{ Nm}$
Environment 2	Coulomb	Stribeck	Lugre	Lugre	Stribeck	Lugre
	$F_c = 35 \text{ Nm}$	$F_c = 37 \text{ Nm}$ $F_s = 42 \text{ Nm}$	$F_c = 30 \text{ Nm}$ $F_s = 35 \text{ Nm}$	$F_c = 25 \text{ Nm}$ $F_s = 30 \text{ Nm}$	$F_c = 35 \text{ Nm}$ $F_s = 40 \text{ Nm}$	$F_c = 40 \text{ Nm}$ $F_s = 45 \text{ Nm}$

Step 3: Choose Controller Parameters

Select parameters $K_c = [100, 3200]^T$ and $K_o = [80, 10, 000]^T$. The initial values are set to $\delta(0) = 0, \dot{\delta}(0) = 0, \Theta(0) = [-420, -280, 0, 280, 420], \zeta(0) = 0, \sigma(0) = 0.001, \gamma_1 = 2.2 \times 10^6, \gamma_2 = 0.1, \gamma_3 = 0.0001, \varepsilon = 0.005$. Set $L(s) = s + 3$, then we can obtain $H(s)L(s) = (s + 3)/(s^2 + 80s + 100, 00)$, which is a proper SPR transfer function. Select symmetric positive definite matrices Q_1 and Q_2 : $Q_1 = \begin{bmatrix} 0.01 & -0.002 \\ -0.002 & 1 \end{bmatrix}, Q_2 = \begin{bmatrix} 154 & -0.02 \\ -0.02 & 0.0006 \end{bmatrix}$. After solving Eqs. (23) and (33), the positive definite matrix P_1 and P_2 are $P_1 = \begin{bmatrix} 0.1776 & 0.00005 \\ 0.00005 & 0.00016 \end{bmatrix}, P_2 = \begin{bmatrix} 1.009 & -0.0003 \\ -0.0003 & 0.0001 \end{bmatrix}$.

Step 4: Results and analysis

The desired steering angle is considered as the common sinusoidal signal $\delta_d = 0.3 \sin(0.4t)$. For contrast, the adaptive type-1 fuzzy logic system controller (AT1F-LSC) with the same parameters as the proposed adaptive interval type-2 fuzzy logic system controller (AIT2-FLSC) is established. Its membership functions are the upper bound of the corresponding membership function in the AIT2FLSC. Figure 7 describes the running states of the SbW system in Environment 1. Figure 7a–b displays comparative diagrams of the tracking performance of the SbW system controlled by the proposed AIT2FLSC and the AT1FLSC. It can be seen that the control accuracy of AIT2FLSC is higher than that of AT1FLSC. Figure 7c shows the curves of the estimated angle $\hat{\delta}_f$ and the actual angle δ_f . It verifies the validity of the observer. Figure 7d shows the control torque of the motor assembly module, which reflects the working stability of the proposed controller.

Figure 8 shows the steering angle tracking curve, tracking error, estimated steering angle, and control torque

of the SbW system in Environment 2 with AIT2FLSC and AT1FLSC. The controllers have the same parameters as the controllers in Environment 1. It is further verified that even if the structure of the friction model changes, the proposed method can guarantee the tracking performance of the SbW system.

To better describe the control performance under different control schemes, four quantitative tracking performance indexes are used to evaluate the performance of the proposed friction modeling method and control strategy, i.e., variance, maximum absolute error (MAE), standard deviation (SD), and RMSE. These metrics are measured as follows:

$$\text{Variance} = \frac{1}{p} \sum_{i=1}^p (e(i) - \bar{e})^2, \quad \text{MAE} = \max\{|e(i)|, i = 1, \dots, p\}, \quad \text{SD} = \sqrt{\frac{1}{p} \sum_{i=1}^p (e(i) - \bar{e})^2},$$

and $\text{RMSE} = \sqrt{\frac{1}{p} \sum_{i=1}^p (e(i))^2}$, where p is the number of experimental data elements, \bar{e} is the mean value of the tracking error. Tables 2 and 3 reflect the superiority of the AIT2FLSC over the AT1FLSC more clearly in the above two friction environments. It can be seen from Tables 2 and 3 that the MAE, RMSE, variance, and SD under the AIT2FLSC are smaller than AT1FLSC. The AIT2FLSC can still maintain high control accuracy even if the friction model and parameters change.

To further verify the adaptability of the proposed algorithm, we add some comparisons with the nested adaptive super-twisting sliding mode (NASTSM) controller [2]. For simplicity, the control input of the NAST-SM controller is straightly given

$$u_{\text{NASTSM}} = \frac{J_0}{k} \left[\frac{\tau_{fri}}{J_0} + u_c \right] \tag{59}$$

$$u_c = -\mu |S_{\text{NASTSM}}|^{\frac{1}{2}} \text{sign}(S_{\text{NASTSM}}) + v(t) \tag{60}$$

$$\dot{v}(t) = -h(t) \text{sign}(S_{\text{NASTSM}}) \tag{61}$$

where $\mu > 0$ is to be designed, the sliding variable S_{NASTSM} is defined as $S_{\text{NASTSM}} = \dot{e} + \lambda_1 \cdot e$, the nested adaption laws are shown as follows:

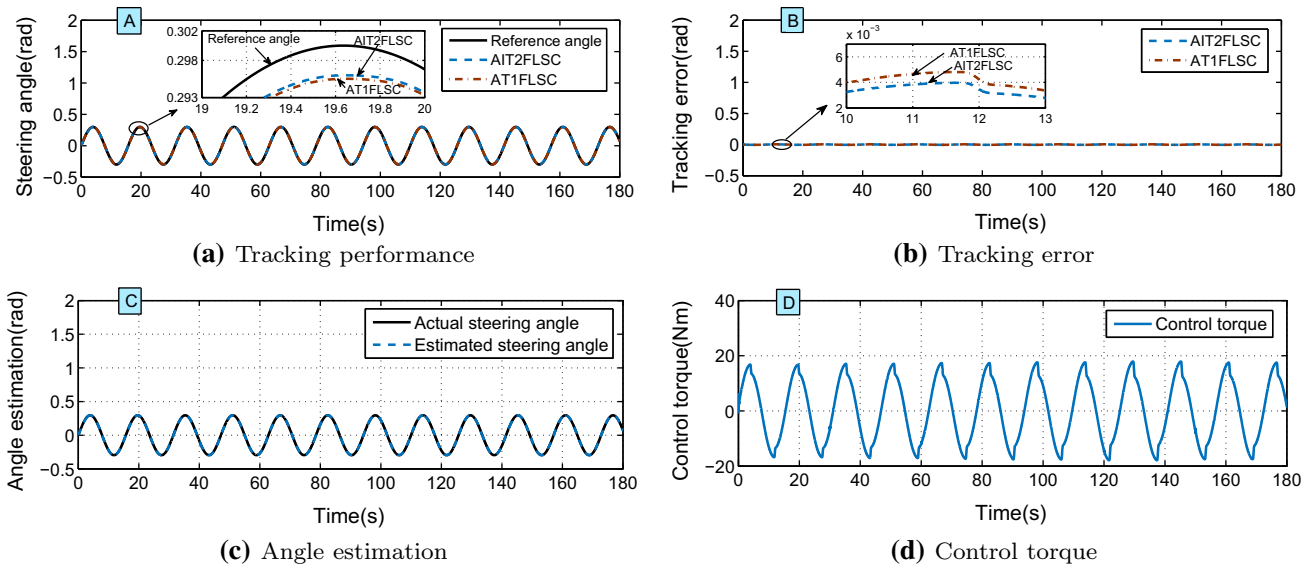


Fig. 7 Simulation diagram of Environment 1

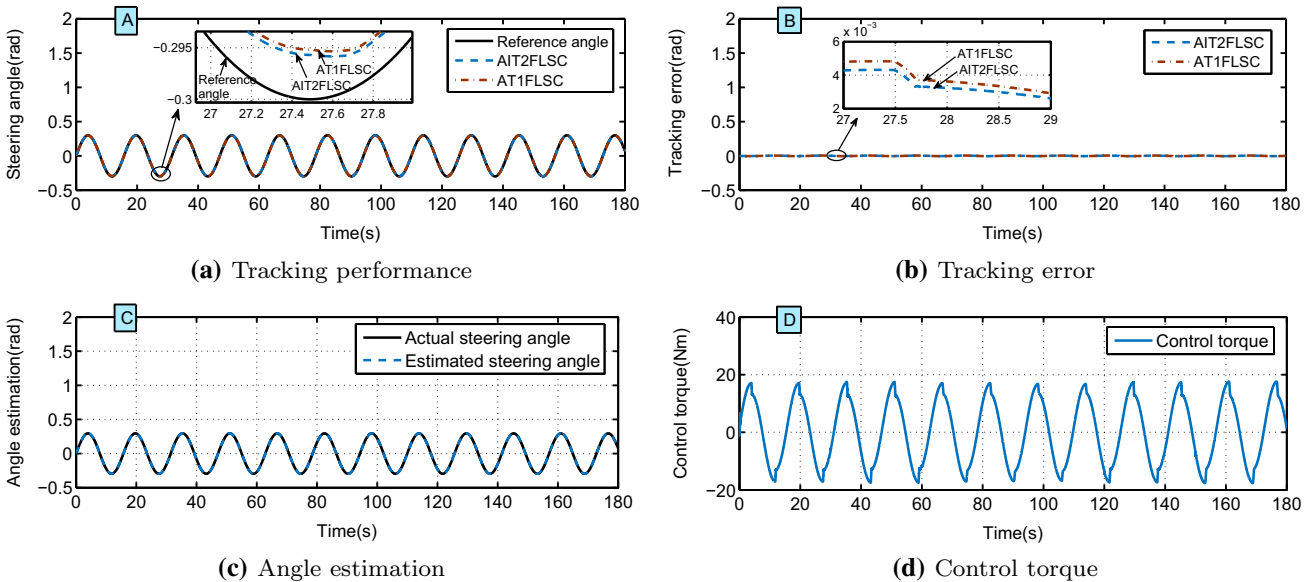


Fig. 8 Simulation diagram of Environment 2

$$\dot{h}(t) = -[\rho_0 + \rho(t)]\text{sign}(g(t)) \tag{62}$$

$$\dot{\rho}(t) = \begin{cases} \omega|g(t)| & \text{if } |g(t)| > g_0 \\ 0 & \text{otherwise} \end{cases} \tag{63}$$

$$g(t) = h(t) - \frac{1}{\zeta}|\bar{\varphi}_{eq}(t)| - o \tag{64}$$

$$\varphi(t) = h(t)\text{sign}(S_{\text{NASTSM}}) \tag{65}$$

$$\dot{\bar{\varphi}}_{eq}(t) = \frac{1}{\epsilon}[\varphi(t) - \bar{\varphi}_{eq}(t)] \tag{66}$$

where $\mu = 20$, $\lambda = 2100$, $\rho_0 = 15$, $\omega = 10$, $g_0 = 5$, $\zeta = 0.9$, $o = 1$, and $\epsilon = 1$.

The following two friction environments (Table 4) are set up in the simulation to show the adaptivity of the controller designed in this paper. Figure 9 describes the comparative diagrams of the tracking performance controlled by the NASTSM controller and the proposed AIT2FLSC in Case 1. From Fig. 9b, we can find that the tracking performance of both controllers is similar between 0 and 100 s. The NASTSM controller and AIT2FLSC can achieve similar control results, which indicates that the NASTSM controller parameters have been optimized. However, once the friction parameters change in between 100 and 200 s, the superiority of AIT2FLSC can be clearly demonstrated. Figure 10 shows the comparison effect in

Table 2 Standard performance indexes of Environment 1

Time	$t \in [0, 30]s$	$t \in (30, 60]s$	$t \in (60, 90]s$	$t \in (90, 120]s$	$t \in (120, 150]s$	$t \in (150, 180]s$
MAE						
AT1FLSC	$4.81E^{-3}$	$4.79E^{-3}$	$4.81E^{-3}$	$4.86E^{-3}$	$4.91E^{-3}$	$4.80E^{-3}$
AIT2FLSC	$4.30E^{-3}$	$4.28E^{-3}$	$4.30E^{-3}$	$4.34E^{-3}$	$4.39E^{-3}$	$4.28E^{-3}$
RSME						
AT1FLSC	$3.12E^{-3}$	$3.10E^{-3}$	$3.05E^{-3}$	$3.03E^{-3}$	$3.13E^{-3}$	$3.16E^{-3}$
AIT2FLSC	$2.79E^{-3}$	$2.76E^{-3}$	$2.72E^{-3}$	$2.70E^{-3}$	$2.79E^{-3}$	$2.81E^{-3}$
Variance						
AT1FLSC	$9.72E^{-6}$	$9.58E^{-6}$	$9.26E^{-6}$	$9.16E^{-6}$	$9.78E^{-6}$	$9.98E^{-6}$
AIT2FLSC	$7.75E^{-6}$	$7.63E^{-6}$	$7.37E^{-6}$	$7.29E^{-6}$	$7.77E^{-6}$	$7.93E^{-6}$
SD						
AT1FLSC	$3.12E^{-3}$	$3.10E^{-3}$	$3.04E^{-3}$	$3.03E^{-3}$	$3.13E^{-3}$	$3.16E^{-3}$
AIT2FLSC	$2.78E^{-3}$	$2.76E^{-3}$	$2.71E^{-3}$	$2.70E^{-3}$	$2.79E^{-3}$	$2.82E^{-3}$

Table 3 Standard performance indexes of Environment 2

Time	$t \in [0, 30]s$	$t \in (30, 60]s$	$t \in (60, 90]s$	$t \in (90, 120]s$	$t \in (120, 150]s$	$t \in (150, 180]s$
MAE						
AT1FLSC	$4.88E^{-3}$	$4.89E^{-3}$	$4.73E^{-3}$	$4.70E^{-3}$	$4.77E^{-3}$	$4.82E^{-3}$
AIT2FLSC	$4.36E^{-3}$	$4.37E^{-3}$	$4.23E^{-3}$	$4.20E^{-3}$	$4.26E^{-3}$	$4.30E^{-3}$
RSME						
AT1FLSC	$3.13E^{-3}$	$3.11E^{-3}$	$3.02E^{-3}$	$2.98E^{-3}$	$3.06E^{-3}$	$3.17E^{-3}$
AIT2FLSC	$2.80E^{-3}$	$2.77E^{-3}$	$2.70E^{-3}$	$2.66E^{-3}$	$2.73E^{-3}$	$2.82E^{-3}$
Variance						
AT1FLSC	$9.78E^{-6}$	$9.66E^{-6}$	$9.12E^{-6}$	$8.84E^{-6}$	$9.37E^{-6}$	$1.0E^{-5}$
AIT2FLSC	$7.80E^{-6}$	$7.70E^{-6}$	$7.26E^{-6}$	$7.03E^{-6}$	$7.45E^{-6}$	$7.97E^{-6}$
SD						
AT1FLSC	$3.13E^{-3}$	$3.11E^{-3}$	$3.02E^{-3}$	$2.97E^{-3}$	$3.06E^{-3}$	$3.17E^{-3}$
AIT2FLSC	$2.79E^{-3}$	$2.77E^{-3}$	$2.69E^{-3}$	$2.65E^{-3}$	$2.73E^{-3}$	$2.82E^{-3}$

friction case 2. It further illustrates that even if the friction structure and parameters change simultaneously, the designed controller can still maintain a superior control effect. The design of the NASTSM controller depends on the accurate friction torque, while the proposed AIT2FLSC is based on the friction modeling method of adaptive interval type-2 fuzzy logic system. Therefore, when the friction structure and parameters change during the control process, the designed adaptive controller can quickly adjust so that the influence of control accuracy caused by the friction uncertainty can be reduced. Based on the above simulation comparisons, it can be seen that the proposed friction compensation control strategy achieves better control performance.

Table 4 Friction environment for comparison between AIT2FLSC and NASTSM controller

	Friction model $\tau_{fric}(t/s)$	
	$t \in [0, 100]s$	$t \in (100, 200]s$
Case 1	Coulomb $F_c = 10 \text{ Nm}$	Coulomb $F_c = 200 \text{ Nm}$
Case 2	Coulomb $F_c = 10 \text{ Nm}$	Lugre $F_c = 200 \text{ Nm}$ $F_s = 205 \text{ Nm}$

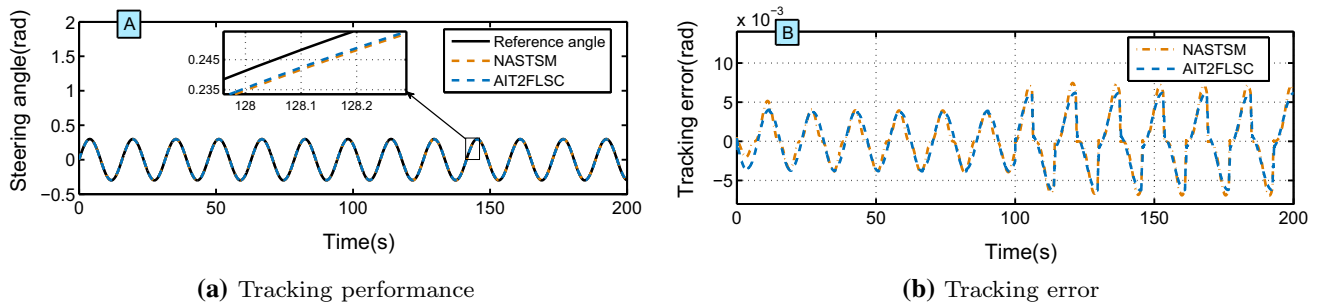


Fig. 9 Comparison results of AIT2FLSC and NASTSM controller in Case 1

6 Experimental results

To further demonstrate the practical control performance of the proposed controller for the SbW system, hardware-in-loop (HIL) experiment verifications are implemented.

Step 1: Build experimental platform

The HIL experimental platform of the SbW system is shown in Fig. 11. In this experimental platform, the dSPACE-DS1202 device is used as the control unit of the SbW system, and a servo motor driver (XinJE DS2-20P7) is used for driving a steering motor (XinJE MS80ST-M02430B-20P7) equipped with a reducer. Firstly, the steering angle δ_f of the front wheels is measured by a linear sensor (KTF-100) fixed on the steering arm. Then, the steering angle δ_f is transmitted to DS1202 equipped with a dual-core 2 GHz PowerPC micro-controller with 16-bit D/A converters. Finally, the output voltage signal computed by DS1202 is converted into the control input of the steering motor by the driver. dSPACE upper computer system can monitor the related variables of the SbW system by interface soft (ControlDesk). Noise and interference will cause the measurement error of the sensor, so the angle signal is processed by the Kalman filter ($x_0 = 0, P_0 = 15, A = 1, B = 0, C = 1, D = 0, Q = 0.04, R = 15$).

Step 2: Establish IT2 FLS system

Set the fuzzy rules as shown in Eq. (58), then the following membership functions of \tilde{A}_1^j and \tilde{A}_2^j are selected as

follows: $\bar{\mu}_{A_1^1}(\hat{e}) = 1/(1 + \exp((3 \times (\hat{e} - 0.4))))$, $\underline{\mu}_{A_1^1}(\hat{e}) = 1/(1 + \exp((3 \times (\hat{e} - 0.2))))$; $\bar{\mu}_{A_1^2}(\hat{e}) = \exp(-0.2 \times (\hat{e} + 0.01)^2)$, $\underline{\mu}_{A_1^2}(\hat{e}) = \exp(-0.3 \times (\hat{e} + 0.01)^2)$; $\bar{\mu}_{A_1^3}(\hat{e}) = \exp(-0.2 \times \hat{e}^2)$, $\underline{\mu}_{A_1^3}(\hat{e}) = \exp(-0.3 \times \hat{e}^2)$; $\bar{\mu}_{A_1^4}(\hat{e}) = \exp(-0.2 \times (\hat{e} - 0.01)^2)$, $\underline{\mu}_{A_1^4}(\hat{e}) = \exp(-0.3 \times (\hat{e} - 0.01)^2)$; $\bar{\mu}_{A_1^5}(\hat{e}) = 1/(1 + \exp((-3 \times (\hat{e} + 0.4))))$, $\underline{\mu}_{A_1^5}(\hat{e}) = 1/(1 + \exp((-3 \times (\hat{e} + 0.2))))$.

Step 3: Choose controller parameters

Select parameters $K_c = [40, 130]^T$ and $K_o = [8, 1000]^T$. The initial values are set to $\delta(0) = 0$, $\hat{e}(0) = 0$, $\Theta(0) = [-500, -250, 0, 250, 500]$, $\zeta(0) = 0$, $\gamma_1 = 25,000$, $\gamma_2 = 0.0001$, $\gamma_3 = 0.0001$, $\varepsilon = 0.1$, $\sigma(0) = 0.0001$. Set $L(s) = s + 3$, then we can obtain $H(s)L(s) = (s + 3)/(s^2 + 8s + 1000)$, which is a proper SPR transfer function. Select symmetric positive definite matrices Q_1 and Q_2 :

$$Q_1 = \begin{bmatrix} 0.01 & -0.005 \\ -0.005 & 0.25 \end{bmatrix}, \quad Q_2 = \begin{bmatrix} 10.144 & -0.033 \\ -0.033 & 0.006 \end{bmatrix}$$

After solving Eqs. (23) and (33), the positive definite matrix P_1 and P_2 are

$$P_1 = \begin{bmatrix} 0.0597 & 0.0001 \\ 0.0001 & 0.001 \end{bmatrix}, \quad P_2 = \begin{bmatrix} 1.009 & -0.003 \\ -0.003 & 0.001 \end{bmatrix}$$

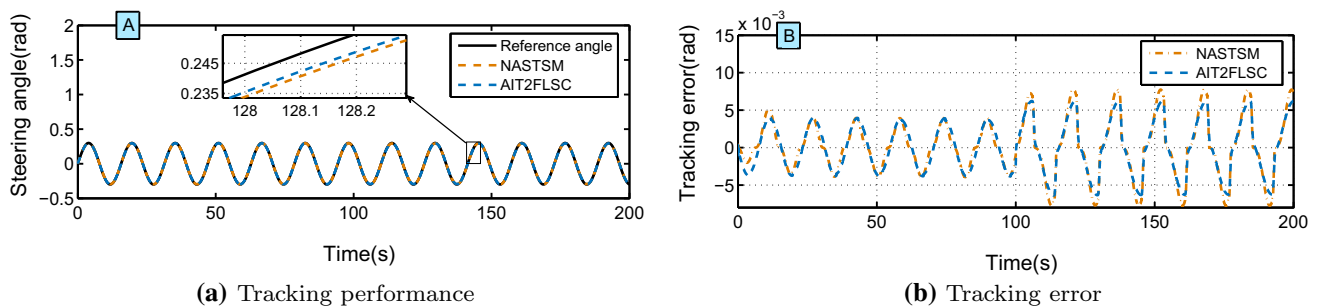
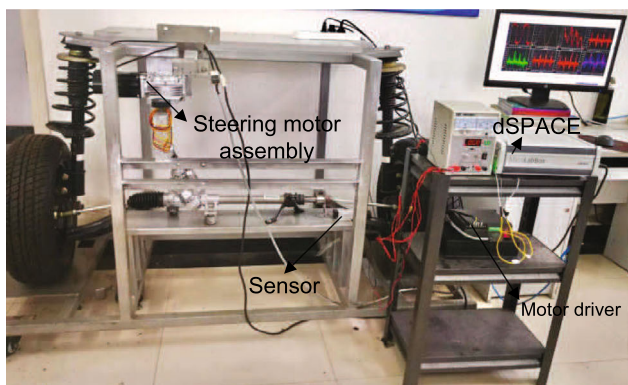
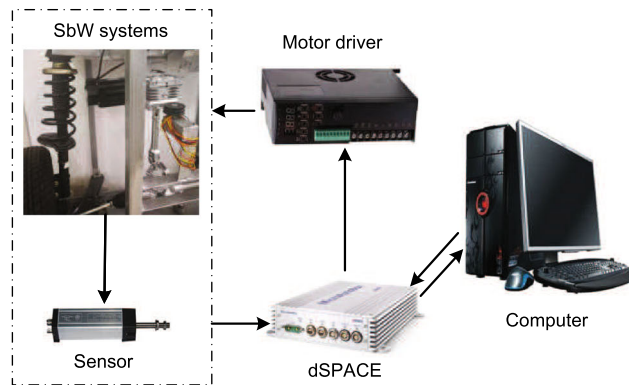


Fig. 10 Comparison results of AIT2FLSC and NASTSM controller in Case 2

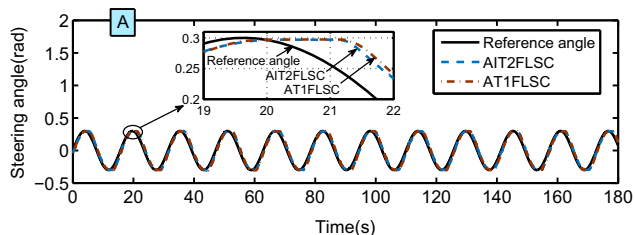


(a) Physical diagram of experimental platform

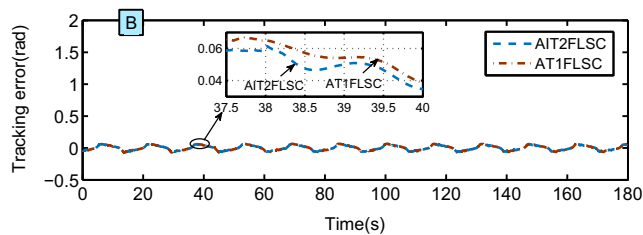


(b) Schematic diagram of experimental platform

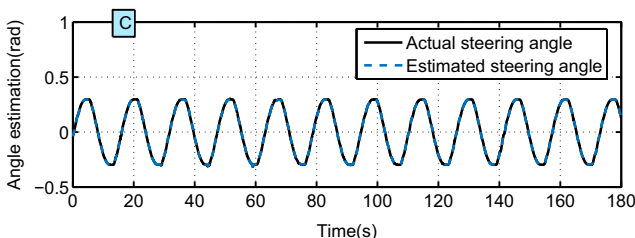
Fig. 11 The HIL experimental platform



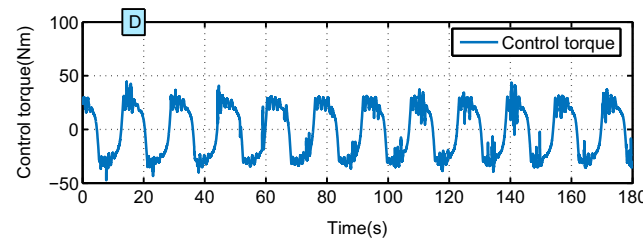
(a) Tracking performance



(b) Tracking error



(c) Angle estimation



(d) Control torque

Fig. 12 Experimental results of sine curve

Step 4: Results and analysis

To further verify the effectiveness of the designed controller, we carried out experimental verification under two target paths of sine curve and step signal.

Case I: Sine curve

The effectiveness and superiority of the proposed control strategy are verified in Fig. 12. Figure 12a, b display the performance comparison under the proposed AIT2FLSC and AT1FLSC. We can see the control accuracy of AIT2FLSC is higher than that of AT1FLSC. The trajectories of the front wheels’ steering angle and the steering angle estimation are shown in Fig. 12c. It can be seen that the designed observer can accurately estimate the front wheels’ steering angle. Figure 12d shows the control torque of the motor assembly module, which reflects the working stability of AIT2FLSC.

The obtained numeric values of the performance metrics are displayed in Table 5. As it is revealed, the control performance obtained from the designed AIT2-FLSC is superior than the one obtained from AT1FLSC. The MAE, RMSE, variance, SD under the AIT2FLSC are 0.0652 rad, 0.0111 rad, 0.0014 rad, and 0.0368 rad, respectively, which is less than AT1FLSC (0.0718 rad, 0.0142 rad, 0.0017 rad, and 0.0407 rad).

Case II: Step signal

The target steering angle is shown in Fig. 13, which is switched between 0.3 and - 0.3 rad at $t = 53, 124, 233, 304$ s. Figure 14 and Table 6 illustrate the adaptability of the proposed AIT2FLSC when compared with the AT1FLSC. At 53 s, the steering angle regulation time of the AIT2FLSC is 4.21 s, which is 5.41 s for the AT1FLSC. The overshoot of the AIT2FLSC is

Table 5 Standard performance indexes of experimental results

Indexes	MAE	RSME	Variance	SD
AIT2FLSC	6.52 E⁻²	1.11 E⁻²	1.4 E⁻³	3.68 E⁻²
AT1FLSC	7.18E ⁻²	1.42E ⁻²	1.7E ⁻³	4.07E ⁻²

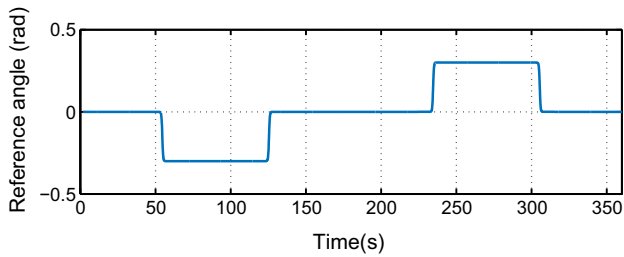
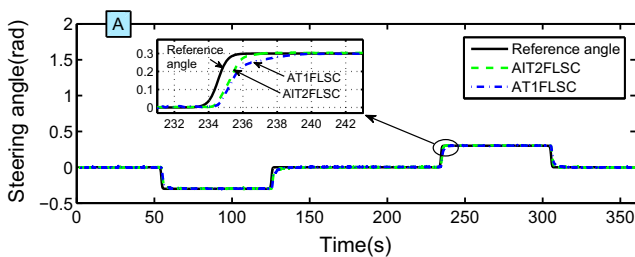
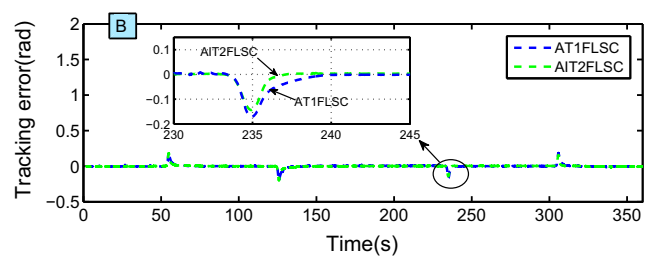


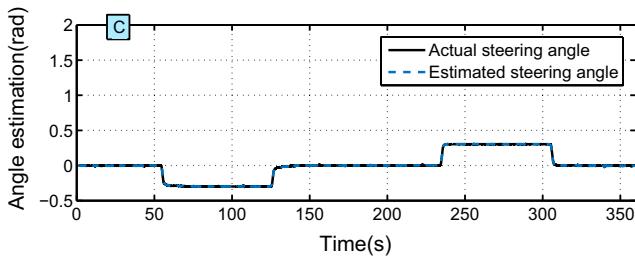
Fig. 13 Step signal



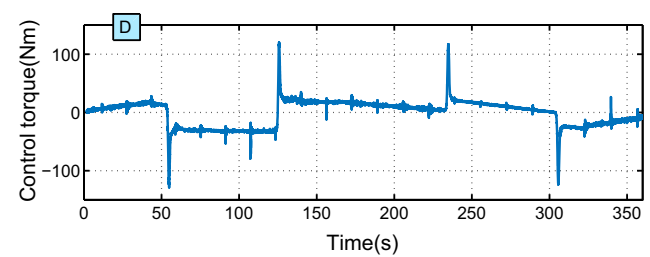
(a) Tracking performance



(b) Tracking error



(c) Angle estimation



(d) Control torque

Fig. 14 Tracking performance of step signal

Table 6 Standard performance indexes of step signal

Switching time	Control method	Overshoot (rad)	Settling time (s)
53 s 0 ~ -0.3 rad	AT1FLSC	0.1952	5.41
	AIT2FLSC	0.1826	4.21
124 s -0.3 ~ 0 rad	AT1FLSC	0.2128	5.93
	AIT2FLSC	0.1975	5.03
233 s 0 ~ 0.3 rad	AT1FLSC	0.1724	5
	AIT2FLSC	0.1437	2.91
304 s 0.3 ~ 0 rad	AT1FLSC	0.185	4.7
	AIT2FLSC	0.1586	3

0.1826 rad, which is less than that of the AT1FLSC (0.2532 rad). Furthermore, at 124 s, the AIT2FLSC still has the shortest settling time, it is about 5.03 s. For the AT1FLSC, the regulation time is 5.93 s. Moreover, the overshoot for the AIT2FLSC is 0.1975 rad, which is smaller than the AT1FLSC (0.2128 rad). Thus, it's verified that the proposed AIT2FLSC still shows a better steering angle dynamic response compared with the AT1FLSC. More comparative results can be found in Table 6. Figure 14c shows the trajectories of the front wheels' steering angle and the steering angle estimation. It can be seen that the designed observer can accurately estimate the front wheels' steering angle. Figure 14d shows the control torque of the motor assembly module, which reflects the working stability of AIT2FLSC.

7 Conclusions

An observer-based adaptive interval type-2 fuzzy logic system controller is proposed for the adverse influence of the friction torque on the SbW system. It has been proven theoretically that

the proposed controller can make the front wheels' steering angle accurately track the target signal. Simulations and experimental results have demonstrated the effectiveness and adaptability of the proposed modeling and control method.

The three main points of conclusions in the presented work can be summarized as follows: (1) an observer is designed to estimate the angular velocity which can reduce the system sensitivity to measurement noise, the complexity of the structure, and save hardware cost; (2) an AIT2FLSC, which does not require the accurate model of the friction torque, is designed to ensure high steering accuracy of the SbW system; (3) the adaptive IT2 FLS has been used to model the friction torque, in which the exact model is difficult to obtain.

Based on this study, the following researches are worthy of further study:

1. There exists a number of type-2 fuzzy membership functions in the literature, such as Gaussian, sigmoid, triangular, trapezoidal, ellipsoidal, and pi-shaped. In this paper, Gaussian membership functions and sigmoid membership functions are chosen in the design of IT2 FLS. In the future research, we will explore the modeling characteristics of IT2 FLS with different membership functions.
2. In the next step, we will build a vehicle collision avoidance system that includes both path planning and steering control technologies. When the vehicle is driving on a path with obstacles, a collision-free path will be generated by path planning strategy. Then, the vehicle tracks the planned path by controlling the steering front wheels accurately.

Abbreviations δ_{sm} : Steering motor assembly rotational angle; δ_f : Front wheels' steering angle; B_{sm} : Viscous friction coefficient of steering motor assembly; B_e : Viscous friction coefficient of equivalent system; J_{sm} : Rotational inertia of steering motor assembly; J_f : Rotational inertia of front wheels; J_e : Rotational inertia of equivalent system; τ_{sm} : Control torque of steering motor assembly; τ_{12} : Load torque of steering motor assembly; τ_f : Driving torque of front wheels; τ_e : Self-aligning torque of front wheels; τ_{fric} : Friction torque of front wheels; k : Steering motor assembly angle/front wheels angle; F_c : Coulomb friction torque of front wheels; F_s : Static friction torque of front wheels; v_s : Stribeck velocity of front wheels; σ_0 : Stiffness coefficient of bristles; σ_1 : Damping coefficient of bristles; σ_2 : Viscous friction coefficient of front wheels; $g(\delta_f)$: Stribeck effect of front wheels

List of symbols SbW: Steer-by-wire; T1 FS: Type-1 fuzzy set; T2 FS: Type-2 fuzzy set; IT2 FS: Interval type-2 fuzzy set; IT2 FSs: Interval type-2 fuzzy sets; KM: Karnik-Mendel; SPR: Strict positive real; FOU: Footprint of uncertainty; UMF: Upper membership function; LMF: Lower membership function; MAE: Maximum absolute error; RMSE: Root mean square error; SD: Standard deviation; GMS: Generalized Maxwell-slip; RBFN: Radial basis function network; FLS: Fuzzy logic system; HIL: hardware-in-loop; T1 FLS: Type-1 fuzzy logic system; T1 FLSs: Type-1 fuzzy logic systems; T2 FLSs: Type-2 fuzzy logic systems; IT2 FLS: Interval type-2 fuzzy logic system; IT2 FLSs: Interval type-2 fuzzy logic systems; GT2 FLSs: Generalized type-2 fuzzy logic systems; IT2-TSK-FLS: Interval type-2 Takagi-Sugeno-Kang fuzzy logic system; AT1FLSC: Adaptive Type-1 fuzzy logic system controller; AIT2FLSC: Adaptive Interval type-2 fuzzy logic system controller NASTSM Nested Adaptive Super-twisting Sliding Mode

Acknowledgements This work was supported in part by the National Natural Science Foundation of China under Grant 51775103, in part by the State Key Lab of Digital Manufacturing Equipment & Technology under Grant DMETKF2020015.

Compliance with ethical standards

Conflict of interest The authors declared that they have no conflicts of interest to this work. We declare that we do not have any commercial or associative interest that represents a conflict of interest in connection with the work submitted.

References

1. Chuei R, Cao Z (2020) Extreme learning machine-based super-twisting repetitive control for aperiodic disturbance, parameter uncertainty, friction, and backlash compensations of a brushless DC servo motor. *Neural Comput Appl* 32:14483–14495
2. Sun Z, Zheng JC, Man ZH, Fu MY, Lu RQ (2019) Nested adaptive super-twisting sliding mode control design for a vehicle steer-by-wire system. *Mech Syst Signal Process* 122:658–672
3. Wang H, Man ZH, Kong HF, Zhao Y, Yu M, Cao ZW, Zheng JC, Do MT (2016) Design and implementation of adaptive terminal sliding-mode control on a steer-by-wire equipped road vehicle. *IEEE Trans Ind Electr* 63(9):5774–5785
4. Dahl PR (1976) Solid friction damping of mechanical vibrations. *AIAA J* 14(12):1675–1682
5. Wit CCD, Olsson H, Astrom KJ, Lischinsky P (1995) A new model for control of systems with friction. *IEEE Trans Autom Control* 40:419–425
6. Lampaert V, Swevers J, Al-Bender F (2002) Modification of the leuven integrated friction model structure. *IEEE Trans Automatic Control* 47(4):683–687

7. Al-Bender F, Lampaert V, Swevers J (2005) The generalized maxwell-slip model: a novel model for friction simulation and compensation. *IEEE Trans Automatic Control* 50(11):1883–1887
8. Jamaludin Z, Brussel HV, Swevers J (2009) Friction compensation of an xy feed table using friction-model-based feedforward and an inverse-model-based disturbance observer. *IEEE Trans Ind Electr* 56(10):3848–3853
9. Maeda Y, Iwasaki M (2014) Mode switching feedback compensation considering rolling friction characteristics for fast and precise positioning. *IEEE Trans Ind Electr* 61(2):1123–1132
10. Freidovich L, Robertsson A, Shiriaev A, Johansson R (2010) Lugre-model-based friction compensation. *IEEE Trans Control Syst Technol* 18(1):194–200
11. Yao JY, Deng WX, Jiao ZX (2015) Adaptive control of hydraulic actuators with lugre model-based friction compensation. *IEEE Trans Ind Electr* 62(10):6469–6477
12. Wang XJ, Wang SP (2012) High performance adaptive control of mechanical servo system with lugre friction model: Identification and compensation. *J Dyn Syst Meas Control* 34:011021
13. Hidalgo MC, Garcia C (2017) Friction compensation in control valves: nonlinear control and usual approaches. *Control Eng Practice* 58:42–53
14. Sobczyk MR, Gervini VI, Perondi EA, Cunha MAB (2016) A continuous version of the LuGre friction model applied to the adaptive control of a pneumatic servo system. *J Franklin Instit* 353(13):3021–3039
15. Lyshevski SE (2017) Control of high-precision direct-drive mechatronic servos: tracking control with adaptive friction estimation and compensation. *Mechatronics* 43:1–5
16. Tarasov V, Tan H, Jarfors AEW, Seifeddine S (2020) Fuzzy logic-based modelling of yield strength of as-cast A356 alloy. *Neural Comput Appl* 32:5833–5844
17. Khan MJ, Mathew L (2019) Fuzzy logic controller-based MPPT for hybrid photo-voltaic/wind/fuel cell power system. *Neural Comput Appl* 31:6331–6344
18. Mishra AK, Ray PK, Mallick RK, Mohanty A, Soumya RD (2021) Adaptive fuzzy controlled hybrid shunt active power filter for power quality enhancement. *Neural Comput Appl* 33:1435–1452
19. Wang YF, Wang DH, Chai TY (2011) Extraction and adaptation of fuzzy rules for friction modeling and control compensation. *IEEE Trans Fuzzy Syst* 19:682–693
20. Alavudeen Basha A, Vivekanandan S (2020) A fuzzy-based adaptive multi-input-output scheme in lieu of diabetic and hypertension management for post-operative patients: a human-machine interface approach with its continuum. *Neural Comp Appl*
21. Wang YF, Wang DH, Chai TY (2009) Modeling and control compensation of nonlinear friction using adaptive fuzzy systems. *Mech Syst Signal Process* 23(8):2445–2457
22. Chaoui H, Sicard P (2012) Adaptive fuzzy logic control of permanent magnet synchronous machines with nonlinear friction. *IEEE Trans Ind Electr* 59(2):1123–1133
23. Yang YN, Hua CC, Guan XP (2014) Adaptive fuzzy finite-time coordination control for networked nonlinear bilateral teleoperation system. *IEEE Trans Fuzzy Syst* 22(3):631–641
24. Zhong GL, Shao ZZ, Deng H, Ren JL (2017) Precise position synchronous control for multi-axis servo systems. *IEEE Trans Ind Electr* 64(5):3707–3717
25. Tao XL, Yi JQ, Pu ZQ, Xiong TY (2019) Robust adaptive tracking control for hypersonic vehicle based on interval type-2 fuzzy logic system and small-gain approach. *IEEE Trans Cybern.* <https://doi.org/10.1109/TCYB.2019.2927309>
26. Mendel JM (2014) General type-2 fuzzy logic systems made simple: a tutorial. *IEEE Trans Fuzzy Systems* 22(5):1162–1182
27. Mendel JM, John RI, Liu F (2006) Interval type-2 fuzzy logic systems made simple. *IEEE Trans Fuzzy Syst* 14(6):808–821
28. Dorfeshan Y, Mousavi SM (2020) A novel interval type-2 fuzzy decision model based on two new versions of relative preference relation-based MABAC and WASPAS methods (with an application in aircraft maintenance planning). *Neural Comput Appl* 32:3367–3385
29. Lin C, La V, Le T (2020) DC-DC converters design using a type-2 wavelet fuzzy cerebellar model articulation controller. *Neural Comput Appl* 32:2217–2229
30. Sarabakha A, Fu CH, Kayacan E, Kumbasar T (2018) Type-2 fuzzy logic controllers made even simpler: From design to deployment for uavs. *IEEE Trans Ind Electr* 65(6):5069–5077
31. Wang TC, Tong SC, Yi JQ, Li HY (2015) Adaptive inverse control of cable-driven parallel system based on type-2 fuzzy logic systems. *IEEE Trans Fuzzy Syst* 23(5):1803–1816
32. Antonelli M, Bernardo D, Hagrass H, Marcelloni F (2017) Multiobjective evolutionary optimization of type-2 fuzzy rule-based systems for financial data classification. *IEEE Trans Fuzzy Syst* 25(2):249–264
33. Kim CJ, Chwa D (2015) Obstacle avoidance method for wheeled mobile robots using interval type-2 fuzzy neural network. *IEEE Trans Fuzzy Syst* 23(3):677–687
34. Zarandi MHF, Soltanzadeh S, Mohammadi A, Castillo O (2019) Designing a general type-2 fuzzy expert system for diagnosis of depression. *Appl Soft Comput* 80:329–341
35. Bi YR, Lu XB, Sun Z, Srinivasan D, Sun ZX (2018) Optimal type-2 fuzzy system for arterial traffic signal control. *IEEE Trans Intell Transp Syst* 19(9):3009–3027
36. Luo C, Tan C, Wang XY, Zheng YJ (2019) An evolving recurrent interval type-2 intuitionistic fuzzy neural network for online learning and time series prediction. *Appl Soft Comput* 78:150–163
37. Wang Y, Luo C (2019) Online evolving interval type-2 intuitionistic fuzzy lstm-neural networks for regression problems. *IEEE Access* 7:35544–35555
38. Le T, Huynh T, Lin C (2020) Adaptive filter design for active noise cancellation using recurrent type-2 fuzzy brain emotional learning neural network. *Neural Comput Appl* 32:8725–8734
39. Magnis L, Petit N (2016) Angular velocity nonlinear observer from single vector measurements. *IEEE Trans Autom Control* 61(9):2473–2483
40. Levant A (1998) Robust exact differentiation via sliding mode technique. *Automatica* 34(3):379–384
41. Wang H, Man Z, Shen W, Cao Z, Zheng J, Jin J, Tuan DM (2014) Robust control for steer-by-wire systems with partially known dynamics. *IEEE Trans Ind Inf* 10(4):2003–2015
42. Davila J, Fridman L, Levant A (2005) Second-order sliding-mode observer for mechanical systems. *IEEE Trans Autom Control* 50:1785–1789
43. Parka JH, Parkb GT, Kima SH, Moon CJ (2005) Output-feedback control of uncertain nonlinear systems using a self-structuring adaptive fuzzy observer. *Fuzzy Sets Syst* 151:21–42
44. Wu X, Zhang M, Xu M (2019) Active tracking control for steer-by-wire system with disturbance observer. *IEEE Trans Veh Technol* 68(6):5483–5493
45. Do MT, Man ZH, Zhang CS, Wang H, Tay FS (2014) Robust sliding mode-based learning control for steer-by-wire systems in modern vehicles. *IEEE Trans Veh Technol* 63(2):580–590
46. Eshghi A, Mousavi SM, Mohagheghi V (2019) A new interval type-2 fuzzy approach for analyzing and monitoring the performance of megaprojects based on earned value analysis (with a case study). *Neural Comput Appl* 31:5109–5133
47. Mohagheghi V, Mousavi SM (2019) An analysis approach to handle uncertain multi-criteria group decision problems in the

- framework of interval type-2 fuzzy sets theory. *Neural Comput Appl* 31:3543–3557
48. Abdullah L, Zulkifli N (2019) A new DEMATEL method based on interval type-2 fuzzy sets for developing causal relationship of knowledge management criteria. *Neural Comput Appl* 31:4095–4111
 49. Samanta S, Jana DK (2019) A multi-item transportation problem with mode of transportation preference by MCDM method in interval type-2 fuzzy environment. *Neural Comput Appl* 31:605–617
 50. Moody J, Darken CJ (1989) Fast learning in networks of locally-tuned processing units. *Neural Comput* 1(2):281–294
 51. Gaweda AE, Zurada JM (2001) Equivalence between neural networks and fuzzy systems. *Int Joint Conf Neural Netw Washington USA* 2:1334–1339
 52. Jang JSR, Sun CT (1993) Functional equivalence between radial basis function networks and fuzzy inference systems. *IEEE Trans Neural Netw* 4(1):156–159
 53. Li HX, Chen CLP (2000) The equivalence between fuzzy logic systems and feedforward neural networks. *IEEE Trans Neural Netw* 11(2):356–365
 54. Rubio-Solis A, Melin P, Martinez-Hernandez U, Panoutsos G (2019) General type-2 radial basis function neural network: a data-driven fuzzy model. *IEEE Trans Fuzzy Syst* 27(2):333–347
 55. Tong SC, Li HX, Wang W (2004) Observer-based adaptive fuzzy control for SISO nonlinear systems. *Fuzzy Sets Syst* 148(3):355–376
 56. Shi WX (2015) Observer-based fuzzy adaptive control for multi-input multi-output nonlinear systems with a nonsymmetric control gain matrix and unknown control direction. *Fuzzy Sets Syst* 263:1–26
 57. Shi WX (2016) Observer-based indirect adaptive fuzzy control for SISO nonlinear systems with unknown gain sign. *Neurocomputing* 171:1598–1605
 58. Slotine J, Li W (1991) *Applied nonlinear control*. Prentice hall, New Jersey
 59. Tao G (1997) A simple alternative to the Barbalat lemma. *IEEE Trans Autom Control* 42(5):698–698
 60. Van M, Mavrovouniotis M, Ge SS (2019) An adaptive backstepping nonsingular fast terminal sliding mode control for robust fault tolerant control of robot manipulators. *IEEE Trans Syst Man Cybern Syst* 49(7):1448–1458

Publisher's Note Springer Nature remains neutral with regard to jurisdictional claims in published maps and institutional affiliations.